Winter 2012

Waste heat measurement and recovery options in an investment casting process

Patrick Timothy Kilar
University of New Hampshire, Durham

Follow this and additional works at: https://scholars.unh.edu/thesis

WASTE HEAT MEASUREMENT AND RECOVERY OPTIONS IN AN INVESTMENT CASTING PROCESS

BY

PATRICK TIMOTHY KILAR

B.S. in Mechanical Engineering, University of New Hampshire, 2011

THESIS

Submitted to the University of New Hampshire

in Partial Fulfillment of

the Requirements for the Degree of

Masters of Science

in

Mechanical Engineering

December, 2012

UMI Number: 1522313

Dissertation Publishing

UMI 1522313
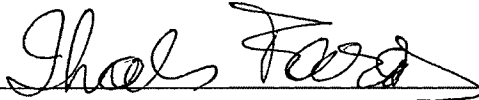
ProQuest LLC
789 East Eisenhower Parkway
P.O. Box 1346
Ann Arbor, MI 48106-1346
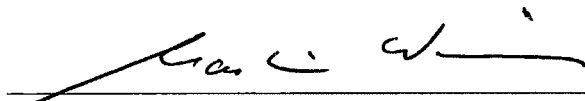
This thesis has been examined and approved.

Brad L. Kinsey

Thesis Co-Director, Brad L. Kinsey, Assoc. Prof, Mechanical Eng. Dept., UNH

Ihab Farag

Thesis Co-Director, Ihab H. Farag, Prof, Chemical Eng. Dept., UNH

Martin Wosnik

Martin Wosnik, Asst. Prof, Mechanical Eng. Dept., UNH

Dec 13, 2012

Date

ii

Contents

DEDICATION

To the cabinet shop.

ACKNOWLEDGEMENTS

LIST OF TABLES

LIST OF FIGURES

ABSTRACT

WASTE HEAT MEASUREMENT AND RECOVERY OPTIONS IN AN
INVESTMENT CASTING PROCESS

by

Patrick Timothy Kilar

University of New Hampshire, December, 2012

In this research, the waste heat emitted from two ovens and a boiler used in the investment casting manufacturing process by New Hampshire based Hitchiner Manufacturing Inc. Co. was determined. This was achieved with measured temperature and standard volume flow rate data gathered from the exhaust stacks using a thermal anemometer. Pressure in the stacks and density were also determined using a differ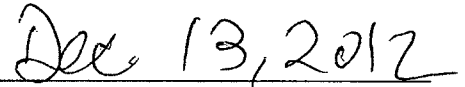ential pressure transducer and combustion analyzer transducer, respectively. The thermal anemometer collected data continuously over a period of 1 week per stack. To support and protect the transducers during the experiments, tripods and enclosures were designed, fabricated and implemented. From the data, economic options to recover the waste heat were analyzed and one was recommended based on the return on investment periods.

CHAPTER I

I. INTRODUCTION

Manufacturing processes and facilities account for approximately 32% of the energy used in the world [1, 2] and 14% of the total energy used in New Hampshire.[3] Automotive, aerospace, defense, and renewable energy industries as well as others continue to innovate and manufacture new products containing ferrous and non-ferrous alloy parts. One means to produce these parts, in addition to machining, forming, powder metallurgy, etc., is through a metal casting process. Over 90 percent of all manufactured goods in the United States contain cast metal components.[4] In this process, molten metal is fed into molds with the desired part geometry and solidifies upon cooling. Due to the temperatures required to melt the metal, casting is an extremely energy intensive process.

There are few if any technical papers in the literature on waste heat recovery in casting. However the Department of Energy has published some related case studies on waste heat recovery in other manufacturing processes. For example, U.S. Steel's plant in Minntac, Minnesota mines and processes iron-bearing rock into pellets for use in steelmaking. There are five production lines at the facility and each has its own kiln, preheater, and dryer which operate at 1,616 K, 1,477 K, and 589 K, respectively. Figure 1 shows typical inputs and outputs for a Sankey flow diagram of an oven. In 2008, U.S. Steel installed an air to air heat exchanger that preheats combustion air in the exhaust stacks exiting the kilns. Through this installation the plant achieved an annual

1

savings of approximately 64.8 GWh, which equates to $1.8 million savings in energy expenses

per year and a return on investment (ROI) of 1.5 years.[5]
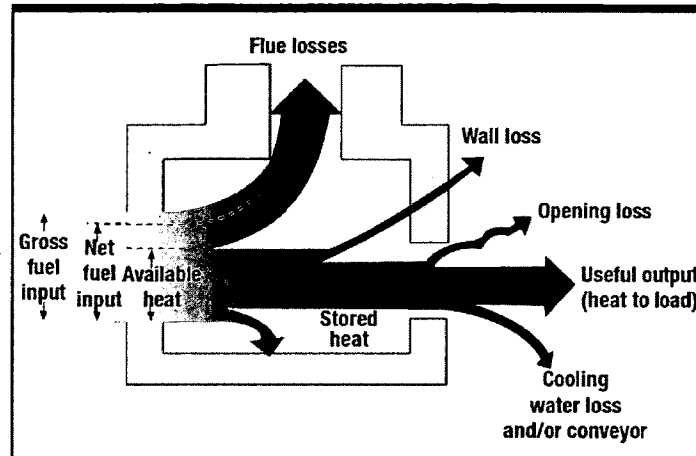
Figure 1. Heat losses in industrial processes.[6]

Additionally waste heat recovery has been studied in the coffee roasting industry.[7] The main

waste heat sources in this process are the natural gas fired coffee roasting ovens. In this study

the temperature and flow rates of exhaust gases exiting from the roasting and cooling stacks of

the existing plant were measured with a resistance temperature detector and a Pitot tube

respectively. The average temperature, waste heat, and standard volume flow rate measured in

the case study were 833.15 K, 454 KW, and 103 SCMM respectively, where SCMM is standard

cubic meters per minute. (More explanation of the units will be given in Chapter III.) The factory

analysis showed that the most beneficial use for the recovered heat was for space heating of

buildings and had an ROI of 7.6 years. [7]

Lastly Shaw Industries, a flooring company, uses a significant amount of steam and warm water

in their processes.[8] An assessment found that waste energy in the water was significant enough

to incorporate a waste water heat exchanger into the stream. Additionally an economizer was

added to the boiler and its pipes were cleaned to increase efficiency. Altogether after implementing heat recovery and other equipment on the boilers $ 872,000 in energy cost savings annually was achieved with an ROI of 1.7 years. [8] In summary manufacturing facilities which use boilers and ovens are excellent candidates for waste heat recovery projects.

Returning to the subject of casting, there are various casting methods, i.e., sand casting, evaporative pattern/lost foam casting, die casting, etc. Table 1 compares various casting processes versus key design and production parameters. [9] Hitchiner Manufacturing Company, Incorporated located in Milford, NH specializes in investment casting of both ferrous and non-ferrous alloys. Investment casting allows for high volume production of light weight, thin walled metal components, which have exceptional surface finish and tight tolerances. It has been estimated that the metal casting industry uses approximately 58.6 to 73.3 TWh annually.[4] Furthermore, the average amount of energy annually used by the ovens (i.e., G and J ovens) and boilers at Hitchiner's Automated Casting Facility (ACF) is 19.6 GWh, which thus makes up 0.02% of the industries total energy consumption.[10] Comparing the corresponding monthly consumption rate to that of the production of New Hampshire's Seabrook power station and residential users it is 0.18% (assuming 1.2 GW power production) and 1,701 homes respectively.[11,12]

Table 1. General characteristics of casting processes.[9]

General Characteristics of Casting Processes

	Sand	Shell	Evaporative pattern	Plaster	Investment	Permanent mold	Die
Typical materials cast	All	All	All	Nonferrous (Al, Mg, Zn, Cu)	All	All	Nonferrous (Al, Mg, Zn, Cu)
Weight (kg):							
minimum	0.01	0.01	0.01	0.01	0.001	0.1	<0.01
maximum	No limit	100+	100+	50+	100+	300	50
Typ. surface finish (R_a in μm)	5–25	1–3	5–25	1–2	0.3–2	2–6	1–2
Porosity[1]	3–5	4–5	3–5	4–5	5	2–3	1–3
Shape complexity[1]	1–2	2–3	1–2	1–2	1	2–3	3–4
Dimensional accuracy[1]	3	2	3	2	1	1	1
Section thickness (mm):							
Minimum	3	2	2	1	1	2	0.5
Maximum	No limit	—	—	—	75	50	12
Typ. dimensional tolerance (mm/mm)	1.6–4 mm (0.25 mm for small parts)	±0.003	—	±0.005–0.010	±0.005	±0.015	±0.001–0.005
Cost[1,2]							
Equipment	3–5	3	2–3	3–5	3–5	2	1
Pattern/die	3–5	2–3	2–3	3–5	2–3	2	1
Labor	1–3	3	3	1–2	1–2	3	5
Typical lead time[2]	Days	Weeks	Weeks	Days	Weeks	Weeks	Weeks–months
Typical production rate[2] (parts/mold-hour)	1–20	5–50	1–20	1–10	1–1000	5–50	2–200
Minimum quantity[2]	1	100	500	10	10	1000	10,000

Notes: 1. Relative rating, from 1 (best) to 5 (worst). For example, die casting has relatively low porosity, mid to low shape complexity, high dimensional accuracy, high and die costs, and low labor costs. These ratings are only general; significant variations can occur, depending on the manufacturing methods used.
2. Approximate values without the use of rapid prototyping technologies.
Source: Data taken from J. A. Schey, *Introduction to Manufacturing Processes*, 3d. ed., McGraw–Hill 2000.

4

There are several steps in the investment casting process (see Fig. 2):

1) Wax replicas of the desired part are created using wax injection into dies.

2) The wax replicas are assembled onto a central wax sprue.

3) The ceramic shells are created over the wax assembly by immersing it in a liquid slurry and then in a fine sand.

    i) This process is repeated multiple times to create thick walled ceramic shell.

    ii) The assembly with its ceramic coatings then dries and hardens in humidity controlled rooms maintained by a boiler.

4) In the "Dewax/Burnout" step, the now hardened ceramic shells are placed in a boiler oven to melt out the inner wax assembly and then an oven to remove any residual wax and fire the ceramic mold to receive the molten metal.

5) The ceramic shell is then filled by molten metal via Hitchiner's exclusive counter gravity process instead of the traditional gravity pouring technique. Thus, the sprue does not solidify which is more material efficient and eliminates the process of cutting parts from the sprue.

6) After the metal has cooled and solidified, the ceramic shell is removed by vibration or water jet.

7) For investment casting processes with a solidified sprue, the individual castings are cut from the sprue.

8) Operations such as sanding or grinding are performed to finish the product.

5
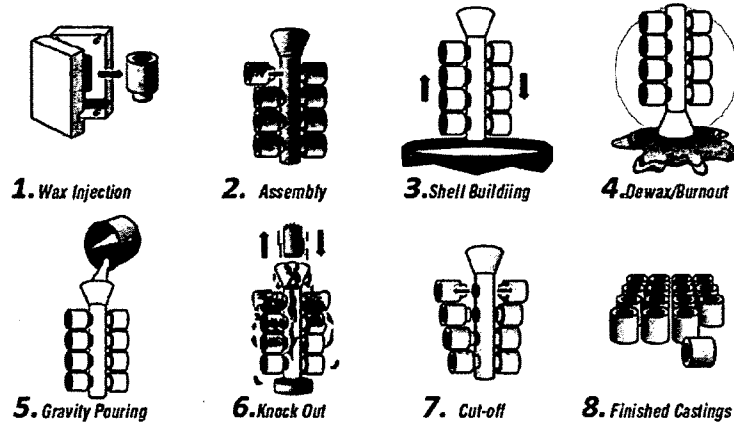
Figure 2. Investment casting process.[13]

The most energy intensive stages in investment casting are the shell building and Dewax/Burnout which use natural gas fired ovens and boilers. The bi-products of natural gas and air's combustion are exhausted to atmosphere (i.e., exhaust losses in Fig. 1) after the thermal energy has been used in the process. Boilers and ovens exhaust these bi-products to the atmosphere and when they have a higher temperature than the surrounding ambient air it exhausts to, it is considered waste heat. According to a report by the Department of Energy (DOE) published in 2011, exhausted thermal energy from industrial operations in metals industries represents 20% to 50% of the total energy used in manufacturing plants, and it is possible to reduce or recover 30% to 60% of the available exhaust thermal energy by using conventional and readily available technologies.[14] The waste heat recovery technology that is the best-fit for the specific investment casting processes used by Hitchiner has been the topic of both internal and external energy efficiency audits.

Generally, waste heat recovery options are most economically viable when the exhausted thermal emission has a consistently high average temperature and flow rate. At ACF two boilers operate 24 hours a day for 7 days a week to maintain humidity control of the mold storage room (i.e., Step 3 in Fig. 2). Humidity control is important so the shells do not lose their shape and/or

6

crack, which would result in a scrap part. Two ovens named the G-oven and J-oven both generally operate 24 hours a day for 4 days a week to prepare the ceramic shells to receive the molten metal and burn out excess wax from the molds (i.e., Step 4 in Fig. 2). Within Appendix III there is an architectural floor plan of ACF and photos of the exhaust stacks from the G-oven, J-oven and the boilers. Note that there are a lot of additional thermal losses in the process (see Fig. 1) but the others are considerably less significant and are more difficult to recover (i.e. their relative magnitudes given by the thickness of the arrows). Therefore, waste heat in this research is considered to be the "exhaust losses" (or stack losses) in Fig. 1.

The three stacks that emit from both the G-oven and J-oven are referred to as the afterburner zone, zone 2, and zone 3 stacks. The afterburner zone uses an inductor to pull air/smoke from the oven through a set of burners positioned above the oven that eliminate any volatile organic compounds (VOCs) and hazardous air pollutants (HAPs) from the residual wax's burn off. Zones 2 and 3 do not use any inductors to draw air through them or have afterburners. Instead the driving force for the air flow in zones 2 and 3 is due to the temperature difference between the air inside the oven and the outside ambient air. This phenomenon is called natural convection.

Although other studies have been performed to estimate the waste heat emitted in Hitchiner's investment casting processes, none of them have taken measurements of temperature and flow rate over an extended period of time. The specific goals of the project are 1) to determine the magnitude of waste heat from the G-oven, J-oven, and boiler at ACF, and 2) to determine the most beneficial and economical use of the waste heat available. In order to accomplish these goals, sensors to quantify the data for assessing technological options had to be acquired and the

7

procedures to use them had to be developed. The following information will be presented in the proceeding chapters: Chapter 2 explains the selection of sensors, the validation of flow data in a wind tunnel, and the experimental procedure/instrumentation setup on the roof of ACF; Chapter 3 describes the theoretical equations used to quantify the waste heat emitted and the resulting data; Chapter 4 discusses the waste heat recovery options evaluated and assesses the economics and feasibility of implementation; Chapter 5 describes and contrasts previous waste heat studies at Hitchiner; and lastly Chapter 6 contains the conclusions.

CHAPTER II

II. SENSORS AND EXPERIMENTAL PROCEDURE

Several sensors were used in this research to measure the density of air in the stack, natural gas used in the process, fluid flow, and fluid temperature. For example, a combustion analyzer transducer was used to quantify the percent oxygen in the exhaust gas. The percent oxygen measurement is necessary to calculate the density of the exhaust in each stack. Hitchiner has a combustion analyzer, Bacharach Fyrite Pro (Serial No. MZ1020), for waste heat analysis. The Bacharach can operate in stacks with a temperatures below 811 K, thus it was applicable in all of the stacks in this study. However due to material constraints of the sensor it cannot be inserted closer to the burners. Also a NG thermal mass flow meter (model number 9500) made by Thermal Instrument co. was used to approximate the annual energy use of the process equipment. The final sensor required was a flow sensor to measure the flow rate and temperature in the stacks. As this is the critical sensor for the research, a detailed selection process and validation of the sensor was used.

Flow Sensor Selection

The implementation of a flow sensor into a stack is limited by whether the temperature and flow rate are within the range of the sensor. For example, flow measurements can be taken with a pitot tube, however, this pressure sensor is limited by the high temperatures. Table 2 shows the estimated stack temperatures, pressures, and volumetric flow rates of each stack from the G-oven, J-oven, and boiler as well as their diameters that were referenced. This data came from previous studies.[10,15,16] Also Hitchiner requested approximately a week of data collection per stack in order for them to have confidence in the data that is being used to base their decision of whether or not to purchase heat recovery equipment. So the sensor needs the ability to store significant amounts of data.

Table 2. Estimates of stack conditions.

Stack	Diameter, d_1 [mm]	Temperature, $\bar{T}$ [K]	Pressure $\bar{P}$ [Pa]	Volumetric Flow, $\bar{Q}$ [SCMM]
G-oven (A/B)[15]	457.2	771	101,412	74.33
G-oven (Zones 2 and 3)[15]	812.8	450	101,337	171.46
Boiler[10]	558.8	419	101,412	30.55
J-oven (A/B)[16]	355.6	771	101,412	74.33
J-oven (zones 2 and 3)[16]	406.4	450	101,337	171.46

Note: Data from a Hitchiner study[15], Energy Resources Solutions[10], and Kim Hutchinson[16].

It is desirable to have a sensor that can be implemented in all stack diameters (i.e., from 355.6mm (14 inches)-812.8mm (32 inches)) and conditions. Based off an extensive search two sensors were purchased. One is a thermal anemometer, made by KURZ instruments (model number 2440). The second is a single point differential pressure sensor, similar to a Pitot-Static tube, called an Accutube (model number 22L).Table 3 shows that both sensors have comparable accuracies and can measure in the expected operating range of each stack. As is evident from Table 3, a major difference between the sensors is that the Meriam also measures pressure while

KURZ does not. The two sensors were purchased to determine if this parameter affected the results or could be assumed as atmospheric.

Table 3. Flow sensors accuracy and ranges. [17, 18, 19]

KURZ			
	Accuracy	Range	G-oven A/B
Stack Flow Rate, Q [SCMM]	+/- 1 %	450.12	74
Stack Temperature, T [K]	+/- 5	255 - 771	498
Stack Pressure, P [Pa]	NA	NA	101,412
Meriam			
	Accuracy	Range	G-oven A/B
Stack Flow Rate, Q [SCMM]	+/- 1 %	Flows except 24 - 3.6	74
Stack Temperature, T [K]	+/- 0.9	255-922	498
Stack Pressure, P [Pa]	+/- 0.1%	0-3,447,378	101,412

The KURZ consists of two instruments that work together to collect data on the stack volume flow rate and temperature. One is a thermal anemometer rod which is inserted into the exhaust. The second is a data logger which contains the circuitry to convert the signal to flow and temperature measurements. A picture of the thermal anemometer rod and the data logger is shown in Figure 3.
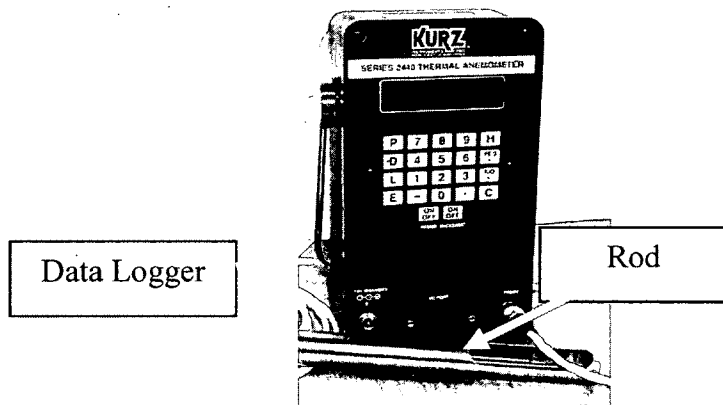
Figure 3. KURZ 2440 interface and anemometer. [17]

The thermal anemometer rod consists of two resistance temperature detectors (RTD); one RTD is heated 50-100 K above the ambient, while the other monitors the ambient. The current required to keep the RTD element heated at different flows is the parameter calibrated in

11

KURZ's wind tunnels. In order to process this signal, a wire exits the end of the thermal anemometer rod and connects to the data logger. The data logger converts the signal into flow rate and temperature values that are saved on its internal memory. The data can be later transferred to a computer through a program called HyperTerminal as a ".txt" file. The KURZ interface can measure 2,300 samples before the data needs to be downloaded. At that time it overwrites the oldest saved data sample. The minimum and maximum programmable time between sampling is 1 and 999 seconds respectively. To achieve the 24/7 data, samples were measured every 100 seconds and the data was downloaded halfway through the week (to assure no important data features were missed).

The Meriam Accutube model 22L is similar to a pitot-static tube in that it senses the differential pressure (i.e., the difference between the high and low pressure ports). Figure 4 shows (A) the hardware and (B) the corresponding sensor model number EJX910A which uses membranes to measure the differential pressure.

(A)   (B)
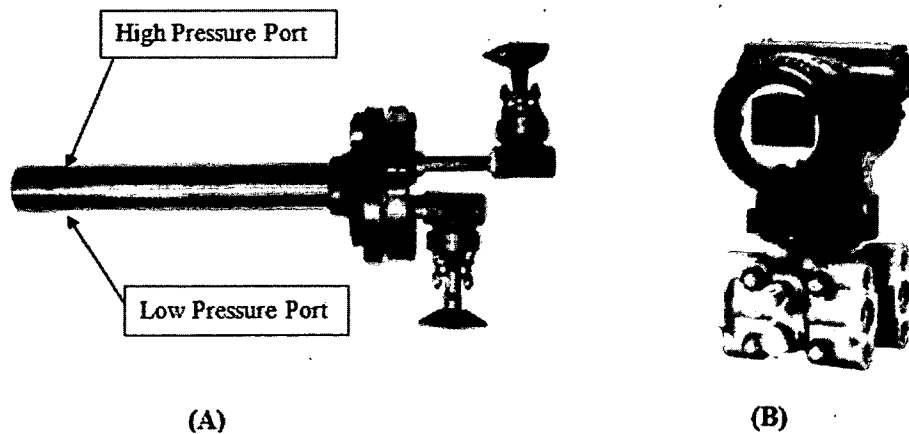
Figure 4. Meriam Accutube (A) hardware and (B) sensor. [20]

These respective high and low pressure ports of the hardware are piped to the sensor via two 12.7 mm (0.5 inch) diameter tubes connected by compression fittings. The length of the tubing is

selected based on the estimated stack exhaust temperature. Therefore, depending on whether the exhaust temperature was closer to either 771 K (i.e., the G-oven or J-oven afterburner stacks) or 419 K (i.e., boiler stack), 4.57 m (15ft) or 1.52 m (5ft) lengths were used. This was done to cool the air prior to the sensor which had an input temperature limit of 393 K. For data logging, a National Instruments data acquisition board (NI 6341), LabView software/program, and a laptop computer was used for continuous sampling.

Flow Sensor Validation

As previously noted two sensors were purchased for this research. Again the principal difference between the two transducers is that the Accutube flow calculation is related to the pressure in the stack and the KURZ calculates flow without a direct measurement of stack pressure (i.e., assumes atmospheric pressure). Because the pressures in the stacks were unknown when purchasing, both sensors were acquired. It was desired to test both sensors in a controlled setting before implementation at Hitchiner for comparison to each other and to assure knowledge of sensor function. The UNH wind tunnel (see Figure 5) was used for this testing, and measurements were taken at wind tunnel speeds within the range of the exhaust gases. The velocity results of the two sensors were compared between each other and with a pitot-static tube in the wind tunnel to evaluate the closeness in data between the two sensors. In order to calculate the waste heat from the process, the velocity of the flow is required as this is used to determine the mass flow rate.
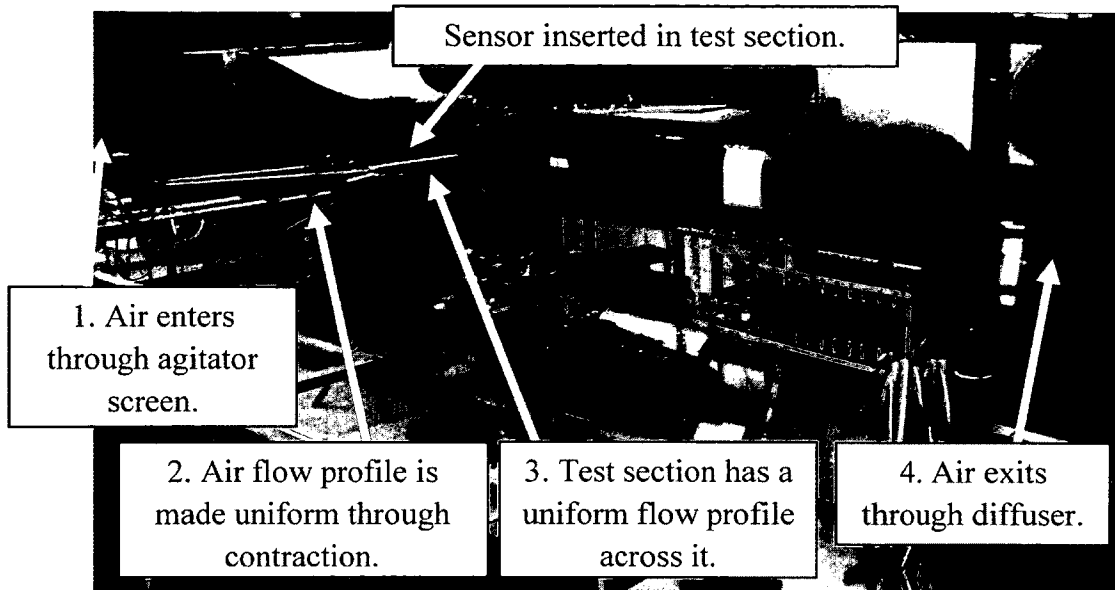
Figure 5. UNH wind tunnel.

Air enters the wind tunnel through an agitator screen to induce turbulence (1). Next the air is accelerated and made into a flat uniform flow profile through the contraction into the test area (2). This makes the velocity uniform across the wind tunnel test area (3). The test area walls are made of clear 19.05 mm (0.75 inches) thickness plexi-glass with interior dimensions of 914.4 mm (36 inches) in length by 457.2 mm (18 inches) in both width and height. Sensors were inserted in the side of the wind tunnel through an opening fabricated for these sensors (see Fig.6). Exiting the test section the system air decelerates and regains static pressure by passing through a diffuser (4). Flow then continues through the fan and air is exhausted into the atmosphere completing the air's cycle through the wind tunnel. The air velocity of the wind tunnel in the test section can range from 3 m/s to 65 m/s. For these tests, the speed of the wind tunnel was varied in 15 increments from its minimum of 3 m/s to a velocity near 22 m/s to correspond to stack flow rates. The following provides the theoretical calculations of flow velocity for the Accutube and pitot-static tube.

14

Theoretical Calculations

Accutube and Pitot-Static Tube. Fluid dynamic assumptions in this wind tunnel analysis include incompressible flow, steady flow, and that Bernoulli's equation is valid. Bernoulli's equation states the sum of the kinetic and potential energy in a fluid along a streamline is the same at all points on that streamline. A streamline is defined as a line that is parallel to the direction of fluid flow at a given instant in time. The general form of Bernoulli's equation is by:

(1)

$$\frac{U_x^2}{2} + gz + \frac{P_x}{\rho} = \text{constant},$$

where U_x is the fluid velocity [m/s] at point x on the streamline, g is the acceleration [m/s^2] due to gravity (assumed to be 9.81 m/s^2), z is the distance [m] of point x with respect to a reference plane, P_x is the pressure [Pa] at point x, and ρ is the density [kg/m^3] of the fluid at all points because of incompressibility. Since Eq. 1 is a constant it can be applied at two locations in a flow to determine, the velocity or pressure at one location if the information is known at the other. Because the ports of the Accutube are horizontal (i.e., at the same z distance, there is no potential energy term, gz). Figure 6 shows a representation of a streamline approaching the Accutube.
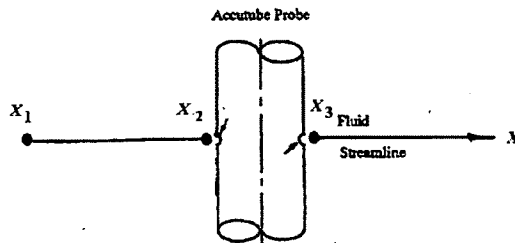
Figure 6. Accutube probe and fluid streamline. [21]

Applying Bernoulli's equation between points X_1-X_2 (note that point X_2 is a stagnant point where V_2 is equal to zero) and X_1-X_3 in Figure 6 and designating air as the fluid the pressure at points 2 and 3 may be represented by:

15

$$P_{x_2} = P_{x_1} + \frac{\rho U_{x_1}^2}{2},$$

$$P_{x_3} = P_{x_1} + \frac{B_1 \rho U_{x_1}^2}{2},$$

where B_1 is a constant that can be determined experimentally. Physically, the B_1 term is due to the wake and shedding effects that occur as the streamline passes over the circular Accutube. [21] The differential pressure (ΔP) [Pa] between the ports of the Accutube is measured by the pressure transducer. Therefore, the ΔP can be represented as the difference between these pressures by:

$$\Delta P = P_{x_2} - P_{x_3} = (1 + B_1)\frac{\rho U_{x_1}^2}{2}.$$

Allowing $B_2 = (1 + B_1)$ and solving Eq. (4 in terms of velocity yields:

$$U_{x_1} = \sqrt{\frac{2\Delta P}{B_2 \rho}}.$$

The working fluid will be air thus in Eq. 2-5 $\rho = \rho_{air}$ which can be mathematically determined by:

$$\rho_{air} = \frac{P_{static}}{R T_{x_1}},$$

where P_{static} is atmospheric pressure [Pa] (101,325 Pascal's), R is the specific gas constant [J/kg-K] (287.06 J/kg-K), and Tx_1 is the absolute air temperature [K] of the ambient air. As mentioned terms B_1 and B_2 are unknown and can be measured experimentally, and the velocity across the test section of the wind tunnel is theoretically uniform. In order to have a separate measurement of velocity allowing the determination of constants B_1 and B_2, a pitot-static tube was inserted upstream of the Accutube into the test section that is connected to a vertical tube manometer. By

combining the known density of the wind tunnel fluid (ρ_{air}), velocity (U_{x1}) calculated by the pitot-static tube together with Bernoulli's equation, and ΔP measured by the transducer, the constant B_2 is given by:

(7)

$$B_2 = \frac{\rho U_{x_1}^2}{2\Delta P}.$$

The following will detail how U_{x1} was calculated using the pitot-static tube and vertical manometer to solve for B_2.

Design standards dictate that the tip of a pitot-static tube must be within 15 degrees of the direction of the flow. A protractor was used to perform this alignment during validation experiments. Again, similar to the Accutube two pressures are sensed by the pitot-static tube at its stagnation and static taps. The differential pressure (DP) is the difference in pressure between these two columns. Vertical tube manometers (filled with water) were connected to the respective pressure outlets of the pitot-static tube. The height of the water in the column increases as the pressure increases. The vertical distance between the height of the static and stagnation water columns was measured using calipers. The measured difference in height, l, [m] between the stagnation and static water columns was converted to pressure by:

(8)

$$DP = \left(P_{stagnation} - P_{static}\right) = \rho_{H2O}\, g l,$$

where $P_{stagnation}$ is the stagnation pressure [Pa], P_{static} is the static pressure [Pa], and ρ_{H2O} is the density [kg/m^3] of the water which was the manometer fluid. Further applying Bernoulli's equation to a stream line impacting the pitot-static tube the velocity related to the difference in stagnation and static pressures can be represented by:

$$U_{x_1} = \sqrt{\frac{2\rho_{H2O}gl}{\rho_{air}}}.$$

Substituting the result of Eq. 8 into Eq. 7 allows the constant B_2 to be determined at different wind tunnel settings by combining it together with the DP measurement from the pitot tube.

KURZ. The KURZ is a Constant Temperature Anemometer (CTA). As the exhaust temperature changes, the CTA feedback control circuit maintains a constant greater temperature above the heated RTD probe and the ambient fluid temperature. [22] The RTD probes are subject to heat transfer by forced convection when they are inserted in a moving exhaust. The heat loss due to forced convection, H, [W] is given by:

(10)

$$H = hA_{KURZ}(T_F\text{-}T_i),$$

where h is the heat transfer coefficient [W/m^2-K], T_F is the surface temperature of the RTD element [K], and A_{KURZ} is the area of the heated element. The calculation of the heat transfer coefficient, h, is generally quantified by experimental data [W/m^2-K]. The relationship for the forced convection heat transfer coefficient for a cylinder in cross-flow follows the non-dimensional correlation of the Nusselt number, N_{Nu}:

(11)

$$Nu = J(Pr)^m(Re)^n$$

(12)

$$Nu = \frac{hd_{KURZ}}{K} = J\left(\frac{\mu C_p}{K}\right)^m \left(\frac{\rho U d_{KURZ}}{\mu}\right)^n,$$

18

where J is a constant, Pr Prandtl number, Re is the Reynolds number, m and n are coefficients, d_{KURZ} [m] is the sensor diameter, C_p [J/kg-K] is the specific heat of the fluid, K [W/m-K] is the thermal conductivity of the fluid, and μ [kg/m^3] is the fluid viscosity. The quantity ρU is the mass flow rate of the fluid which allows the direct measurement of fluid velocity. KURZ assumes the Prandtl number is approximately 0.7 and does not vary much within the temperature range expected (i.e., 500 K and above) and so it is dropped from the equations (i.e., see Fig. 7 to reference Prandtl number versus Temperature [K] for an ideal gas at atmospheric pressure). [23]
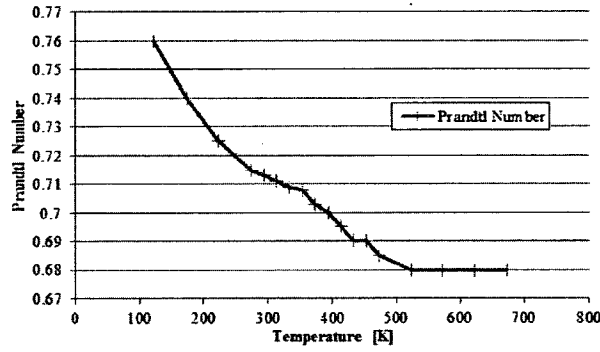
Figure 7. Prandtl number versus temperature [K].[20]

Combining Eqn. 10 and 12, the following result is obtained:

(13)

$$H = \frac{KA_{KURZ}}{d_{KURZ}} \left(\frac{\rho Ud}{\mu}\right)^n (T_F - T_{stack}).$$

This relation allows the two-wire current outputs to be readily converted to an output proportional to mass flow rate. Note that an independent measurement of pressure is not required. Furthermore, KURZ has determined that several other terms affect the heat loss including free convection, radiation, and conduction. KURZ quantifies the total heat loss by all these mechanism by expanding equation 13 by:

(14)

$$H = \frac{KA_{KURZ}}{d_{KURZ}} \left\{ N + D \left(\frac{\rho Vd}{\mu}\right)^n \right\} (T_F - T_{stack}),$$

19

where N and D are constants that account for free convection, radiation, and conduction to the probe support structure. KURZ performs its own sensor calibration in air to ensure its circuitry provides accurate measurements of mass flow rate. In conclusion, all of these calculations are performed internally by the KURZ and its measurements account for several other terms that affect heat loss. Again the sensor does not require independent measurements of pressure.

Results and Discussion

Figure 8Error! Reference source not found. shows the pitot tube velocity versus the Accutube onstant B_2 for various wind tunnel speed settings. These values were obtained in the center of the wind tunnel's test s

avg. B_2 value for
$3.07 < U < 3.14$

avg. B_2 value for
$4.2 < U < 5.6$

avg. B_2 value for
$6.7 < U < 19.8$

B2
B2 Range 1
B2 Range 2
B2 Range 3
Pitot Tube Velocity [m/s]
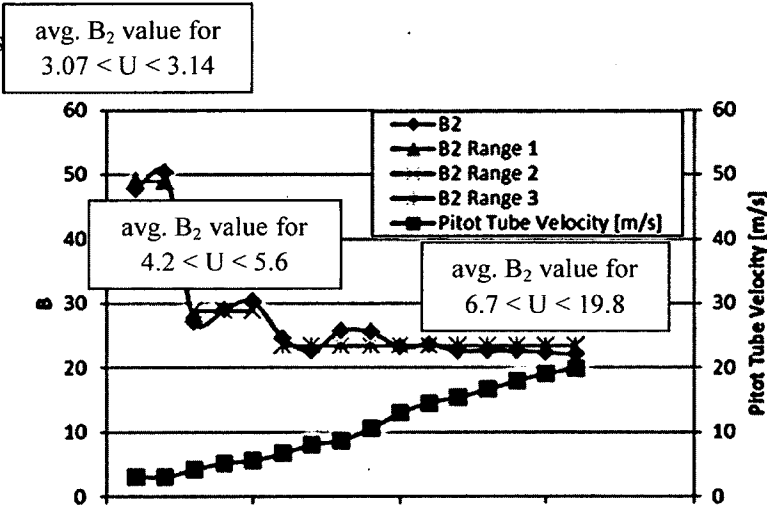
Figure 8. Pitot-static tube velocity and Accutube constant.

There are several values of B_2 present in the data. This was expected because in the ordering of this sensor the salesmen indicated the expected velocity range dictated the constant programmed into the Accutube sensor. The velocity ranges for different B_2 values are indicated in Fig. 8. The maximum percent error in these ranges compared to the data are 1%, 3%, and 5% for increasing velocity ranges. Note that the flow velocity in the stacks is expected to be less than 16 m/s.

20

Further the KURZ thermal anemometer was also inserted in the wind tunnel for the same wind tunnel speed settings. Figure 9 shows the velocity results for the Accutube and KURZ against the velocity of the pitot tube again at the center of the wind tunnel's test section.
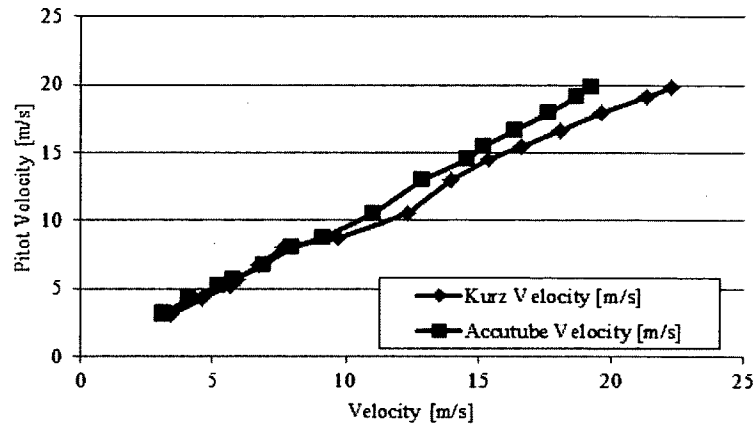
Figure 9. Velocity measurements between flow sensors.

Differences between the Accutube and other flow sensors are due in part to the averaging effect of the B value (three ranges in Fig. 8 using Eqn. 9 and 7). For the KURZ, its differences with the pitot tube and Accutube are due to the Prandtl number assumption, and calibration constant errors (i.e., assumptions of Eq. 14). Again, the pitot tube does not have such assumptions but its sensors cannot withstand the temperatures in the process. The resulting average, maximum, and minimum percent difference between the KURZ and Pitot tube are 7% (i.e., at 13 m/s), 15% (i.e., at 13 m/s), and 1% (i.e., at 5 m/s) respectively. The average percent difference between Accutube and KURZ velocity measurements made in the wind tunnel is 9% with the largest difference being 17%. Based on the wind tunnel tests performed, the accuracy of the two sensors used was deemed to be acceptable

In addition to measurements taken at the center of the wind tunnel's test section, the pitot tube, KURZ, and Accutube were traversed across the wind tunnel. There were no changes in the

output of the transducer. Thus, as expected a uniform flow fluid was obtained across the wind tunnel's test section. This was confirmed at various wind tunnel speed settings.

Experimental Setup and Procedure

Hitchiner's ACF building has a flat rubber roof covered in smooth rocks. The exhaust stacks and their flow are perpendicular to the roofline, and the stacks have a wall thickness of 1.6 mm (0.62 inches). A 31.75 mm (1.25 inches) hole was drilled on the side of a stack to allow sensors to be inserted and aligned perpendicular to the direction of the flow. The sensor was inserted at a height of approximately 1.4 m (4.6 feet) above the roof-line. It was estimated this height is approximately where heat recovery equipment would be positioned. Only one sensor was inserted in a stack at a time. A tape measure with an accuracy of 0.8 mm was used to position the transducer in the center of the stack. This ensured it measured the centerline velocity.

Accutube Set-up

Figure 10 shows the 12.70 mm (0.5 inches) diameter Stainless Steel (SS) piping, 12 Volt direct current (DC) power supply, Accutube sensor, NI DAQ, and Hart Interface Module (HIM) for the Accutube experimental setup.
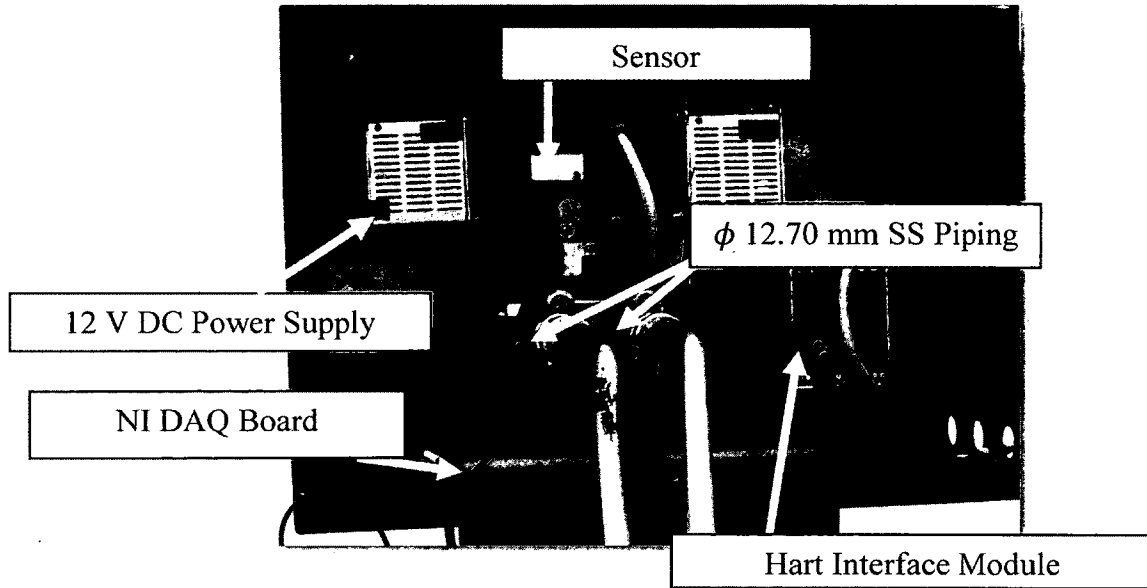
Figure 10. Experimental setup for the DP transducer.

The 12 V DC power supply is required for both the sensor and HIM. The sensor receives the pressure via two 12.70 mm (0.5 inches) diameter SS pipes, and a 100 ohm RTD is also connected to the sensor. The sensor outputs are sent to the HIM, which in turn outputs three 4-20 mA signals proportional to RTD temperature, differential pressure, and static pressure. The wires carrying the three output signals are connected to a NI DAQ board model number 6341. The NI DAQ board is used to log the data on a laptop using LabView. The electronic equipment shown in Figure 10 needed to be protected in order for tests to occur over the period of 24 hours, 7 days a week outdoors on the roof of the building. Figure 11A shows the view of the Accutube and RTD inserted in the stack, through 25.4 mm (1 inch) and 6.35 mm (0.25 inches) diameter shaft collars respectively, and the 12.70 mm diameter SS piping. Figure 12B shows the overall view of the tripods used to support the SS tubing and a 3.05 m (10 feet) square canopy used to protect the Accutube electronics.
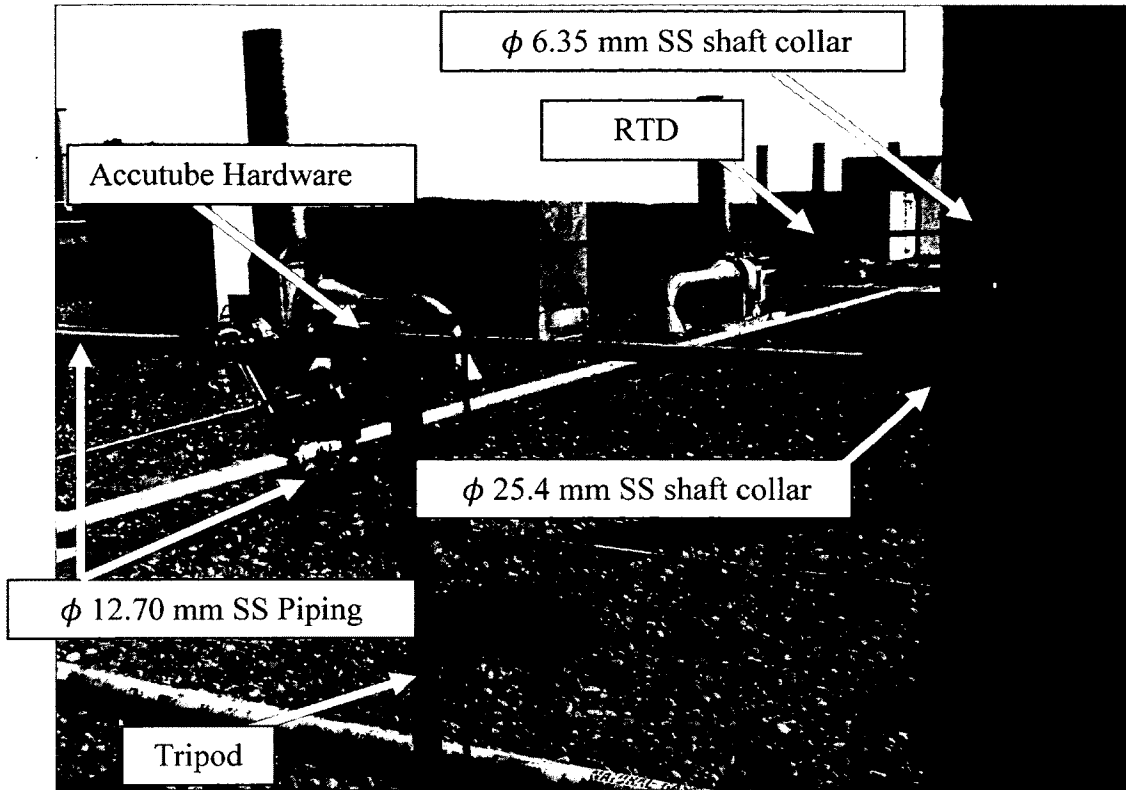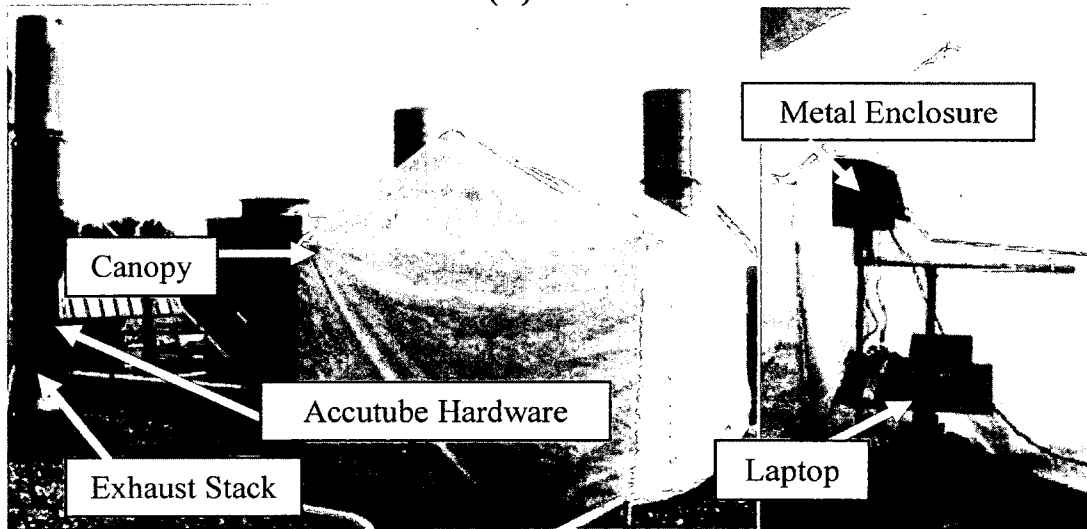
Figure 11. (A) Accutube, (B) outside, and (C) and inside canopy.

The shaft collar was used to firmly fasten the Accutube and RTD sensors at the correct distance into the stack. The tripod allowed the alignment of the Accutube to be adjusted such that it was perpendicular to the direction of exhaust flow. Bubble levels and squares were used in this alignment process with an accuracy of 0.79 mm (0.03 inches). Figure 11C shows the metal

enclosure that contains and protects the electronics shown in Figure 10. The laptop in Figure 11C was used to store the data acquired with the NI DAQ board. A tripod with a desk was used to support the metal enclosure and laptop.

KURZ Set-up

The KURZ requires significantly less components than the Accutube to perform its measurements. Figure 12 shows inside the enclosure used to protect the KURZ interface from the elements.
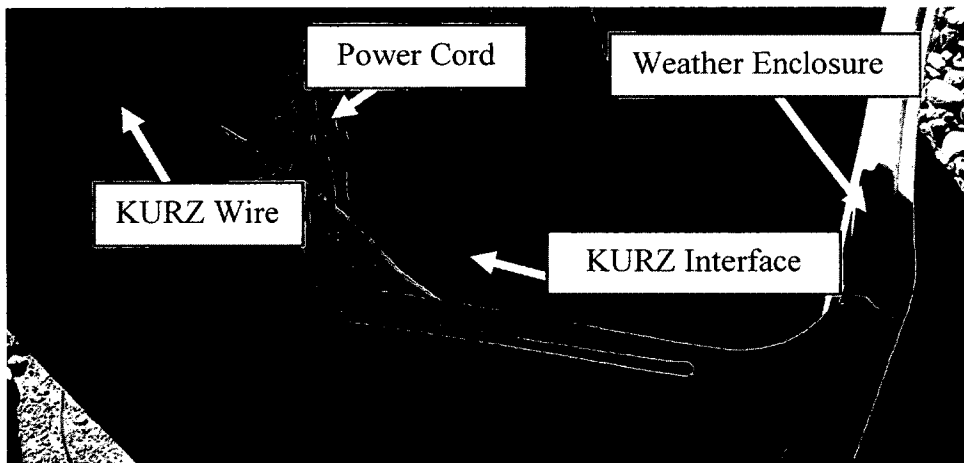
Figure 12. KURZ weather enclosure.

In addition to the larger enclosure the electronic interface was put into a plastic Tupperware container for additional protection. The container top locked close and holes were drilled on its side to allow the power and signal cords to attach to the interface. Figure 13 shows the KURZ thermal anemometer supported by a tripod and inserted into a stack via the same 25.4 mm (1 inch) diameter shaft collar used for the Accutube sensor.
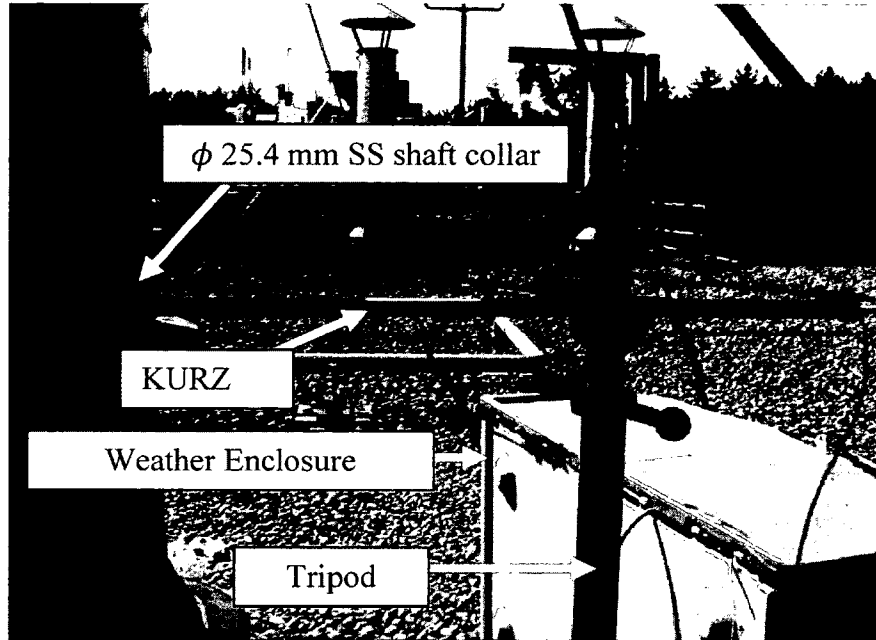
Figure 13. Experimental setup for KURZ.

As with the Accutube, the shaft collar was used to firmly position the KURZ transducer at the center of the stack. Again, the tripod allowed the alignment of the KURZ to be adjusted such that it was perpendicular to the direction of exhaust flow.

Natural Gas Flow Meter

In order to have an accurate measurement of the energy used in the process, natural gas (NG) flow-meters were installed on the G-oven and J-oven. Figure 14. Installed NG transducer. shows the NG flow meter installed via a flange connection to the NG pipeline of the G-oven at ACF. A similar installation was made on the J-oven.
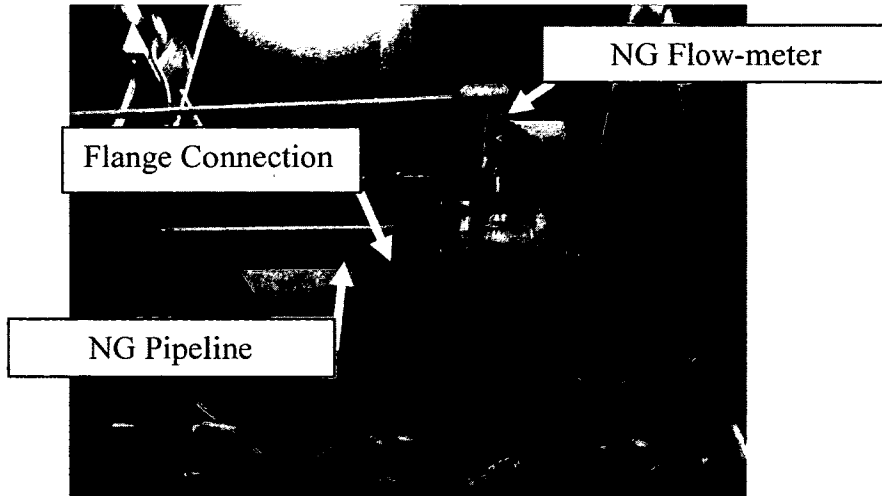
Figure 14. Installed NG transducer.

The NG flow meter measures the volume flow rate [m^3/hr] of NG into the process. The sensor was positioned before the pipes split to each burner. Data was recorded every minute, and 43,200 samples were stored on the data logger until downloaded to a laptop. Once the data logger was filled, no more data was stored or the oldest data was overwritten.

CHAPTER III

III. EQUATIONS AND DATA ANALYSIS

The term "waste heat", E, [W] simply put refers to the waste in the form of a temperature difference between the exhaust gasses and the ambient air that the exhaust stack emits it is calculated by:

(15)

$$E = \rho \, Q \, \big(h(T_{ex}) - h(T_{air})\big),$$

where $h(T_{ex})$ is the enthalpy [J/kg] of the fluid in the stack at atmospheric pressure and its temperature, and $h(T_{air})$ is the enthalpy [J/kg] of ambient air at atmospheric pressure and its temperature. Based on the measurements of the density and pressure, reference tables for air at standard pressure were used to determine the enthalpy.[24] Furthermore since the goal of the study is to quantify the amount of waste heat that is exhausted annually, the ambient temperature will not be measured directly during experimentation. Rather a reference quantity of 294.15 K (21 C) was used for all calculations presented as standard conditions because this was the procedure done by a previous study performed at Hitchiner similarly the flow rate quantity was measured at standard conditions of 293 K and 101.3 kPa.[10,15]

Furthermore, combustion analysis was performed to determine the exhaust gas density. Carbon and hydrogen makeup NG's primary component, methane (CH_4). When combustion occurs with oxygen (O_2) in the air, carbon dioxide (CO_2) and water (H_2O) are the principle chemical products formed. In the stoichiometric (i.e., balanced) reaction, each molecule of methane reacts with two molecules of O_2 producing one molecule of CO_2 and two molecules of H_2O. When this occurs, energy is released as heat as shown by:

(16)

$$CH_4 + 2O_2 => CO_2 + 2H_2O$$
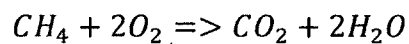
Reactants => Products + Heat

In the actual combustion process other elements are involved such as Nitrogen (N_2). The components in the exhaust have an effect on its density. An industrial handbook was referenced which listed the exhaust gas composition: for nitrogen $N_{2,combustion}$, water vapor $H_2O_{combustion}$, and carbon dioxide $CO_{2,combustion}$ as 7.94, 2.10, and 1.16 cubic meters of air per cubic meters of methane (NG) combusted respectively.[22] Furthermore, to ensure complete combustion of all the NG, an additional stream of air is injected into the burner combustion area. The composition of air is known to be 78.03 vol. % Nitrogen, $N_{2,\%air}$, and 20.99 vol. % Oxygen, $O_{2,\%air}$.[25] This "excess air" adds to the total volume of the exhaust gas by adding more oxygen and nitrogen. Excess air can be defined as the percent air above the amount theoretically needed for complete combustion. In real-world combustion applications, the percentage of excess air, EA, required for gaseous fuels is typically about 15%.[26] The Bacharach combustion analyzers measurement of the percent oxygen $O_{2,Bacharach}$ in the exhaust can be used to calculate the excess air, EA, in the exhaust:

$$\text{(17)}$$

$$EA = \frac{O_{2,Bacharach}}{O_{2,\%air} - O_{2,Bacharach}} \times 100.$$

Further because air consists of N_2 and O_2 their corresponding excess quantities, $N_{2,EA}$ and $O_{2,EA}$ were calculated knowing the percent excess air through:

$$\text{(18)}$$

$$N_{2,EA} = N_{2,combustion} \frac{EA}{100},$$

$$\text{(19)}$$

$$O_{2,EA} = N_{2,EA} \frac{O_{2,\%air}}{N_{2,\%air}}.$$

The stack density at standard conditions $\rho_{stack,standard}$ is calculated by:

$$\text{(20)}$$

$$\rho_{stack,standard} = \frac{\rho_{air,standard} * MW_{stack}}{MW_{air}},$$

where MW_{stack} is the molecular weight of the gas in the stack, MW_{air} is the molecular weight of air, and $\rho_{air,standard}$ is the density of air at standard conditions. Again an industrial handbook was referenced which listed molecular weights for nitrogen MW_{N_2}, water MW_{H_2O}, oxygen MW_{O_2}, carbon dioxide MW_{CO_2}, and air MW_{air} as 28, 18.01, 32, 44.01, and 28.97 respectively. The molecular weight of the exhaust gas was equivalent to the sum of the weights of the components contained in the exhaust multiplied by their percent by volume. The percent by volume of each component varied depending on the amount of excess air calculated by Eqs. 17-20 by:

$$\text{(21)}$$

$$MW_{stack} = \left[\left(\frac{N_{2,combustion} + N_{2,EA}}{TV} * MW_{N_2}\right) + \left(\frac{O_{2,EA}}{TV} * MW_{O_2}\right) + \left(\frac{H_2O_{combustion}}{TV} * MW_{H_2O}\right)\right.$$

$$\left. + \left(\frac{CO_{2,combustion}}{TV} * MW_{CO_2}\right)\right],$$

30

where TV is the total volume in the stack [cubic meters of gas per cubic meters of NG] exhaust given by:

(22)

$$TV = \left(N_{2,combustion} + N_{2,EA}\right) + \left(H_2O_{\,combustion}\right) + \left(O_{2,EA}\right) + \left(CO_{2,combustion}\right).$$

According to our industrial contact at Hitchiner, the boiler operates continuously throughout the year (i.e., 8,766 hours), and both the G-oven and J-oven operate for 51 weeks a year, 4 days a week, or 4,896 hours annually. The ovens do not operate continuously because there are weeks with holidays and scheduled down times associated with maintenance.

Natural Gas Flow Meter

Based on the volume flow rate of NG measured, the average fuel consumption and firing rate were determined. The annual fuel consumption, FC [KWh/year] was determined by:

(23)

$$FC = \frac{Q_{NG}}{EC} * O,$$

where the energy content of NG, EC [m^3/KWh] is 0.0966 m^3/KWh, and Q_{NG} [m^3/hr] is the volume flow rate of NG, and O [hours/year] is the annual hours of operation. Thus, the firing rate FR, is calculated by:

(24)

$$FR = \frac{Q_{NG}/EC}{T},$$

where T [KW] is the maximum heat input rating of the burners listed as listed in the manual (i.e., 3.75 MW for the G-oven).[27] Figure 15 shows the calculated firing rate of the G-oven over a one week period.

31
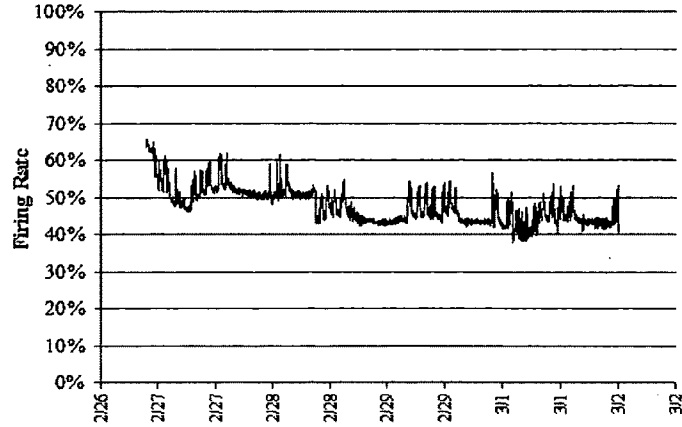
Figure 15. G-oven firing rate.

By averaging the calculated firing rate values over the period of data collection it was determined to be 48%. Therefore the average heat input into the oven was 48% of the total heat input rating of the burners 1.8 MW, which equates to 8,813 MWh/year of energy annually used by the G-oven.

Density Calculation and Pressure Measurement

Error! Reference source not found.4 shows the standard exhaust density from each stack based n the volume percentage of each element calculated from the Bacharach combustion analyzer.

Table 4. Exhaust densities and excess air.

Stack	Density, ρ_{stack}, [kg/m³]	% Difference compare to ρ_{air},	Excess Air, EA %
G-Afterburner	1.18	1.31	350
G-Zone 2	1.19	0.77	1,040
G-Zone 3	1.19	0.57	2,675
J-Afterburner	1.18	0.94	688
J-Zone 2	1.19	0.76	1,100
J-Zone 3	1.19	0.77	1,040

The exhaust gas density does not vary more than 1.31% from the density of air at standard conditions of 1.20 kg/m^3. Note that the excess air measured is considerably more than the industry standard of 15%.[26] One likely cause of this is that draft inducers blow air into the G-oven and J-oven afterburner stacks to cause any smoke in the oven to be pulled through the afterburner stack. Also with all the stacks there is a large gap between the stacks connected to the oven and the fume hood which exhausts through the roof as shown in Figure 16. Finally by design car bottom ovens have no bottom to prevent air from leaking into the oven. It is speculated based on these factors significant excess air is introduced into the exhaust flow which leads to the density of the exhaust being close to air and the corresponding considerable excess air measurements. Attempts were made to substantiate this however by taking density measurements in the large gap shown in Fig. 16 however the Bacharach transducer could not operate at the temperature in excess of 538 C (i.e., 1000 F).
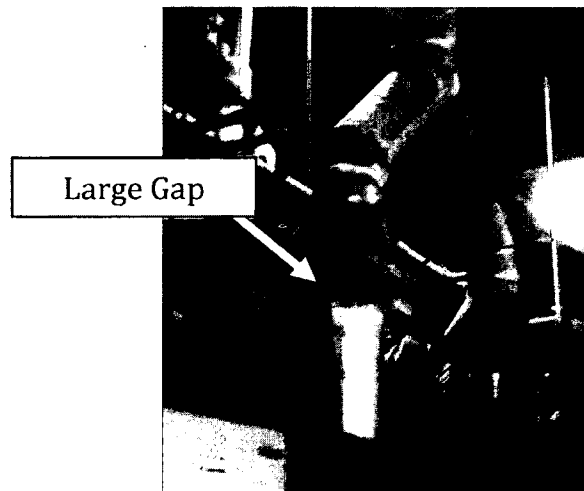
Figure 16. Natural convection stacks and their fume hoods.

The pressure measured in the G-oven and J-oven afterburner stacks are both 101,249 Pa. The accuracy of the measured values is +/-0.1% which is +/-101 Pa. Thus, within the accuracy range of the sensor it is possible that atmospheric pressure (i.e., 1atm=101,325 Pa) is being measured in the stacks. Discussion with the designers/builders of the ovens, ETTER Engineering, indicated

33

the natural convection stacks are at atmospheric pressure, and the afterburner stacks are at a slight vacuum because of the air inductors.[28] Note the KURZ is a thermal mass flow meter that assumes the density of air in its volume flow rate calculation, and based on these measurements uncertainty in measurement caused from density and pressure variation from air at atmospheric pressure was deemed small enough to ignore.

Volume Flow Rate Calculation

The velocity of the exhaust fluid was measured in each exhaust stack using the KURZ. The KURZ instrument was detailed in Chapter II. For analysis exhaust stacks may be conceptualized as a control volume. Control volumes defined with a volume V are the space through which the exhaust fluid travels. Thus the flow rate is described as the amount of fluid which passes its control surfaces. Figure 17 shows a schematic:
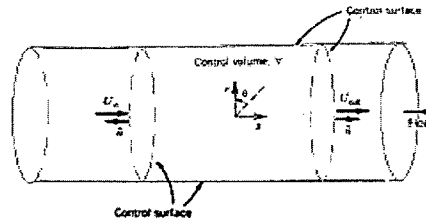
Figure 17. Control volume of a pipe.

The three dimensional velocity field at a point in the exhaust stack control volume in cylindrical coordinates is described by:

(25)

$$\vec{U} = \vec{U}(x, r, \theta) = ue_x + ve_r + we_\theta,$$

where x, r, and θ are unit vectors in each of the component directions x, r, and θ respectively and u, v, and w are the corresponding scalar velocity magnitudes.

34

Another relation which can be used to describe the flow is the conservation of mass equation. Thus, the rate at which mass accumulates within the control volume plus the net flow of mass $\dot{m}$ [kg/s] that physically crosses any of its control surfaces will be zero:

$$\frac{\partial}{\partial t} \iiint_{CV} \rho \, dV + \oiint_{CS} \rho \, \vec{U} \cdot \hat{n} dA = 0, \tag{26}$$

for steady flows, where $\hat{n}$ is the outward normal from a control surface of area A [m^2]:

$$\frac{\partial}{\partial t} \iiint_{CV} \rho \, dV = 0 \tag{27}$$

and

$$\dot{m} = \iint_{A} \rho \, U dA, \tag{28}$$

through each plane perpendicular to the stack axis, so that:

$$\dot{m}_{in} = \dot{m}_{out}. \tag{29}$$

Constant density flows across control surfaces is described in terms of the volume flow rate by:

$$Q = \iint_{A} U dA = \int_{0}^{2\pi} \int_{0}^{r_1} U(r, \theta) r dr d\theta, \tag{30}$$

where equation 29 is applied to circular exhaust stacks, x is the axial position, and r_1 is the exhaust stack radius (see Fig. 19). Using the average velocity $\bar{U}$ [m/s] the volume flow rate is given by:

$$\bar{U} = \frac{1}{A} \iint_{A} U dA, \tag{31}$$

$$Q = \bar{U}A. \tag{32}$$

35

Expanding on identifying the average velocity and flow rate through the control volume an additional classification is whether the flow is either turbulent or laminar. In general turbulent flow is characterized by variation in velocities among other properties as compared to the more orderly laminar flows. Flows are characterized by the dimensionless parameter called the Reynolds number Re by:

(33)

$$Re = \rho \frac{\overline{U}2r_1}{\mu}.$$

In pipes the flow is laminar when Re < 2000. [29] Table 5 shows the average velocities and Re numbers of the respective stacks. The Reynolds numbers calculated for each stack indicate turbulent flows. Additionally the flow magnitudes statistical variation known as its turbulence intensity T.I. is given by:

(34)

$$T.I. = \frac{\sqrt{\frac{1}{N}\Sigma_{i=0}^{N-1}(U_i - \overline{U})^2}}{\overline{U}},$$

where N is the total number of points in the data set, U_i is the instantaneous velocity [m/s], and $\overline{U}$ is the average velocity of the data set [m/s]. Table 5 shows the calculated turbulence intensities for each stack. Note a total of 21 velocity measurements made over 40 minutes where used to calculate the turbulence intensity in each instance. Flow profile warping may occur when measurements are taken at a location where the ratio of length over diameter (i.e., L/D) of straight pipe is small. Note direct distance measurements were not taken due to the logistics of taking them over the equipment and approximations are shown in Table 5. Regarding standards, "Velocity traverses at any cross-sectional location some 20-40 pipe diameters downstream of any pipe fitting in a long section of straight pipe are preferred".[29] It is noted that the L/D ratios of the measurement locations were not within this preferred range. Additionally, the entrance

36

length, L_e [m], defined as the distance downstream from the entrance to the location at which the boundary layers have grown together and the flow is considered fully developed is given by:

(35)

$$L_e = 4.4Re^{1/6}$$

Table 5 shows the entrance length values for all the stacks again these values being greater than the L/D values indicate that measurements were taken in the entrance length of a developing flow profile.

Table 5. Average velocities and Reynolds numbers per stack.

Source	$\bar{U}$ [m/s]	Re	T.I.	L/D	L_e [m]
G Afterburner	5.78	201,646	0.06	10	34
J Afterburner	5.73	140,413	0.06	12.86	32
G Zone 2	3.88	216,977	0.07	5.63	34
G Zone 3	1.78	99,841	0.06	5.63	30
J Zone 2	3.24	90,597	0.02	11.25	29
J Zone 3	2.43	67,956	0.04	11.25	28
Boiler	2.96	113,811	0.05	10.91	31

The G-oven afterburner stack was traversed using the KURZ because of its potential with waste heat recovery equipment (waste heat recovery equipment covered in Chapter IV). The circular exhaust duct was divided along its circumference into equal area concentric rings. The stack was accessed by ports 1, 2, 3, and 4 each spaced 90 degrees from one another in a cross-section of the duct perpendicular to the flow (such that 1 is 180 degrees from 3 and 2 180 degrees from 4). This allowed for 4 measurements to be made in each strip (i.e., ID1-ID5) for a combined total of 20 velocity measurements shown in Table 6.

Table 6. G-oven afterburner velocity traverse data.

IDn	Insertion Depth (mm)	Velocity [m/s]				Average Velocity [m/s]
		Port 1	Port 2	Port 3	Port 4	
ID1	11.94	5.32	5.34	5.38	5.40	5.36
ID2	38.10	5.50	5.63	5.52	5.53	5.54
ID3	67.82	5.57	5.63	5.50	5.71	5.60
ID4	105.16	5.56	5.67	5.54	5.69	5.61
ID5	177.55	5.65	5.73	5.60	5.79	5.69

The difference between the average velocity of ID2 and ID5 is only 3%. The strip with the greatest average velocity is the one closest to the center of the stack (i.e., ID5). Note considerable variation in velocity measurements within a strip were observed with a maximum percent difference of measurements within strip ID1 thru ID5 of 1%, 2%, 4%, 3%, and 3% respectively. The closeness of the results was deemed acceptable. The average velocities calculated for individual strips (i.e., ID1-ID5) were graphed in Figure 18.
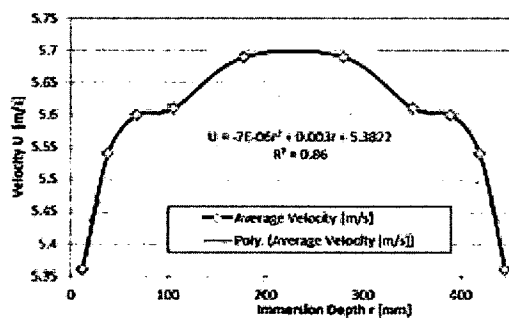
Figure 18. Flow profile in G-oven afterburner stack.

A polynomial trend-line with an exponent of 2 (i.e., a potential fully developed parabola only the equation is displayed on Fig.18) was fit to the data. Reasons the R-squared value is low may be attributed to the flow which was not fully developed (low L_e value and corresponding low L/D value) and the turbulent nature of the flow. The equation was applied to calculate the average velocity of the flow profile. Note experimental measurements were made in the center of the

exhaust stack and to determine an average velocity at that location the ratio of the average and maximum velocity values corresponding to the trend-line (i.e., 5.70 m/s and 5.58 m/s respectively) were used to determine the average value corresponding to the average centerline measurement experimentally attained (i.e., 5.78 m/s) . It was determined to be 5.66 m/s or equivalently 55.72 SCMM. Thus the average velocity is 2% different from the max center-line velocity. Note there is error in the trend-lines flow profile estimate due to the R-squared number being less than 1.

Calculated Waste Heat

Once the atmospheric pressure was measured using the Accutube sensor, no further data was collected due to the difficulties operating this sensor on the roof. The KURZ sensor assumes was positioned in the centerline of the exhaust stack to take measurements. Appendix section III can be referenced to view the raw data that was collected by the KURZ (i.e., volume flow rate [SCMM] and temperature [K], and the calculated waste heat [KW] over the week of experimental data collection).

Note in order to determine if the opening and closing of oven doors would have an effect on the waste heat emitted the data was analyzed. The data sampling rate was generally 1 sample per 100 seconds. At that sampling rate there are no obvious peaks in the data that could be correlated to the opening and closing of the door despite the fact that the opening and closing the door takes approximately 20 seconds. The appendix shows the raw data as it was collected over the week.

Boiler Calculated Waste Heat. Two boilers at ACF operate continuously to provide the steam requirements of the facility (Note they are programed such that they take turns as primary steam providers in a routine known as lead-lag) to generate 1,435 kg/hour of steam at 721.6 kPa. [30] Steam input from the boilers is required in order to control the humidity of the shell building room. Concerning the waste heat generated by this process, each boiler has its own stack that is outfitted with an economizer to reclaim waste heat exhaust which is used to preheat the steam line. The waste heat from one boiler stack is shown in Fig. 19**Error! Reference source not ound.** (Note measurements were taken above the existing economizer and with only one sensor waste heat from the other boiler was not measured).
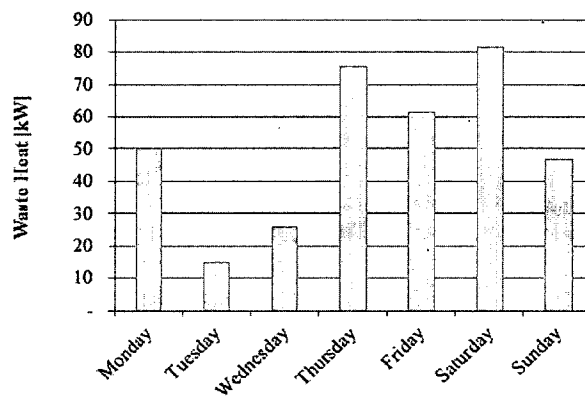
Figure 19. Daily average waste heat exhausted from boiler.

Based on the calculated waste heat from one boiler stack shown in Fig. 19 it is believed that Tuesday and Wednesday the other boiler was primarily leading while Thursday through Sunday and Monday this boiler was primarily leading. The waste heat from both boilers would be the sum of the leading and lagging components. Note that no observations were made to substantiate that the boiler was either leading or lagging during a specific day. Table 7 shows the average temperature, waste heat, and volume flow rate that were emitted from the stack over the 7 days of monitoring.

Table 7. Boiler exhaust average temperature, waste heat, and flow rate.

Temperature, $\overline{T}$ [K]	Waste Heat, $\overline{E}$ [KW]	Flow Rate, $\overline{Q}$ [SCMM]
354	53	36

G-oven Calculated Waste Heat. Again, the G-oven prepares the ceramic casting shells to receive molten metal. Waste heat was measured from the afterburner zone, zone 2, and zone 3 stacks of the oven. The total heating capacity of the oven is 3.75 MW (i.e., oven burners 3.43 MW + afterburners 0.32 MW) note from determining the firing rate was 48% the oven thus operates at 1.8 MW. [27] Figure 20 shows the average waste heat emitted from the G-oven considering all stacks and Table 8 shows the corresponding average temperature, waste heat, and flow rate per stack.

Figure 20. Daily average waste heat exhausted from G-oven.

Table 8. G-oven exhaust average temperature, waste heat, and flow rate.

	Temperature, $\overline{T}$ [K]	Waste Heat, $\overline{E}$ [KW]	Flow Rate, $\overline{Q}$ [SCMM]
afterburner	744.11	576.16-516.58*	56.95-55.72*
zone 2	447.44	375.55	100.73
zone 3	310.26	18.20	45.70

*Note 55.72 SCMM estimated average from traverse.

41

Considering the average firing rate of the oven the waste heat emitted through the exhaust accounts for approximately 50% of the total heat input other sources for heat loss are detailed in Fig. 1. The afterburner stack is at the front of the oven (where product enters). Stacks from zones 2 and 3 are approximately evenly spaced along the length of the oven. Insulation has been inserted in the stack of zone 3 by Hitchiner to retain more heat in the oven. Correspondingly, the exhaust temperature of Zone 3 is significantly lower than the exhaust temperature of zone 2. Lastly, on Wednesday the oven burners were shut down for one shift because there was no available product. Normally there are no shutdowns over the period between Monday-Thursday. Therefore the average casting temperature, waste heat, and flow rate excluded the data from Wednesday.

J-oven Waste Heat. Again, the J-oven has the same function as the G-oven. Figure 21 shows the average waste heat emitted from the J-oven. The total heating capacity of the oven is 1.58 MW (oven burners 1.23 MW + afterburners 0.35 MW) the firing rate was measured from this oven because no natural gas sensors were installed (i.e., G-oven had a 48% firing rate). [31] Waste heat was measured from the afterburner zone, zone 2, and zone 3 stacks. Figure 21 shows the oven operated 24 hours, 4 days a week, Monday through Thursday. Table 9 shows the corresponding average temperature, waste heat, and flow rate during the days of casting (Monday-Thursday).
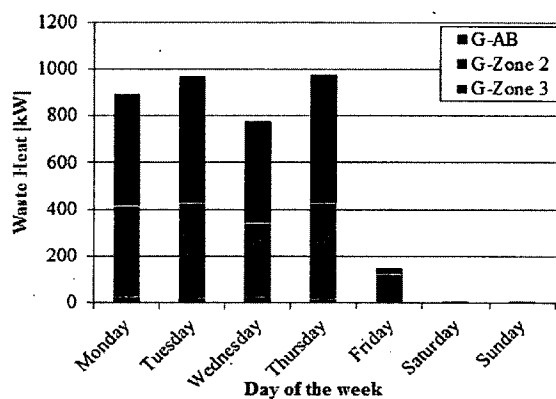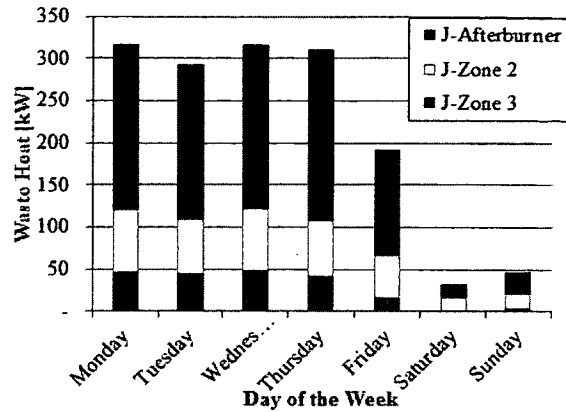
Figure 21. Daily average waste heat exhausted from J-oven.

Table 9. J-oven exhaust average temperature, waste heat, and flow rate.

	Temperature, $\bar{T}$ [K]	Waste Heat, $\bar{E}$ [KW]	Flow Rate, $\bar{Q}$ [SCMM]
afterburner	572.71	193.19	28.30
zone 2	427.44	68.18	20.69
zone 3	414.06	46.01	15.43

Unlike the G-oven, the data from zones 2 and 3 are comparable due to the closeness of the two

stacks (see Fig. 3). In addition, unlike zone 3 of the G-oven no insulation has been inserted in the

stack. Again as stated earlier the firing rate was not measured so comparisons of heat input to

waste heat emitted could not be made.

CHAPTER IV

IV. EVALUATION OF WASTE HEAT RECOVERY OPTIONS

Waste heat recovery is the process of reusing the waste heat in the production process or alternatively converting a portion of it to electricity. By reusing the heat in the process, it will effectively reduce the required fuel input. Alternatively by converting a portion of it into electricity, the waste heat can supplement the electrical demand of a facility. During the period of this analysis in 2011-2012, the delivered electricity and natural gas costs at Hitchiner's ACF facility are approximately \$120/MWh and \$27/MWh respectively. [32] The results of the economic and feasibility analysis of different waste heat recovery options are explained in this chapter.

Waste Heat Recovery Considerations

Using the measured data, companies that offer waste heat recovery technologies were approached considering the sources of waste heat available in this study. If an option could be used to recover waste heat, the corresponding project cost, return on investment (ROI), and carbon reduction were among the general parameters that were calculated for comparison. The

ROI estimates the time in years required for the energy savings of an option to equal the total cost of the option. The ROI [year] can be calculated by:

<div align="right">(36)</div>

$$ROI = \frac{TC - I}{C * S} = \frac{AC}{RV}$$

where TC [USD] is the total cost of the system (i.e., installation and equipment cost), I [USD] is the incentive amount, C [USD/MWh] is the cost of energy, S [MWh/yr] is the estimated annual energy savings, AC [USD] is the actual cost of the option (i.e., the total cost minus the incentive amount), and RV [USD] is revenue from the annual energy savings (i.e., the price of the energy multiplied by the annual energy saved by the option). The incentive (I) is offered by a utility company or government agency for an energy reduction project only for one year. The incentive amount is determined by multiplying the utilities determined incentive rate, IR, [USD/MWh] by the estimated annual energy savings of the respective heat recovery option:

<div align="right">(37)</div>

$$I = IR * S.$$

Incentive programs offered by the State and Federal government and utility companies were thoroughly researched in order to determine the actual cost of implementing a heat recovery option. It was found that renewable energy certificates (REC) are not awarded because waste heat recovery technologies derive their energy from non-renewable technologies. However the money from REC funds a State program through the Regional Greenhouse Gas Initiative (RGGI) called NH Pays 4 Performance, which is in a trial period.[33] The guidelines for the program are not expected to be defined or in operation until the second quarter of 2012.[33] Additionally, Hitchiner's account manager at PSNH, their electricity provider, couldn't derive any incentives on the selected waste heat recovery technologies.[34] Lastly National Grid, Hitchiner's Natural

Gas provider, was contacted. Through National Grid's evaluation of the preheat air to combustion burners option, they determined they could award $68.26/MWh of incentives over the first year the recovery option was implemented.[35] The incentive amount is factored into all the ROIs listed in the proceeding sections.

Several waste heat recovery options were identified and evaluated (listed from the smallest to largest ROI): preheat air to combustion burners, steam generator, organic Rankine cycle, space heating, economizer, thermo-electrics, and combined heat and power. Due to the lower temperature only the economizer was considered for the boiler.

Recovery Options

Waste Heat Recovery Steam Boiler

The waste heat recovery steam generator (WHRSG) option reduces the steam requirements of the boiler. Fig. 22 shows a schematic of the WHRSG where water is pumped into a helical coil heat exchanger installed in-line an exhaust stack then using this heated flow a mechanical separating valve would then direct generated steam to the boiler. Thus, the NG used to create steam by the boilers is decreased.

How Steam Is Produced In A Clayton Heat Recovery Boiler
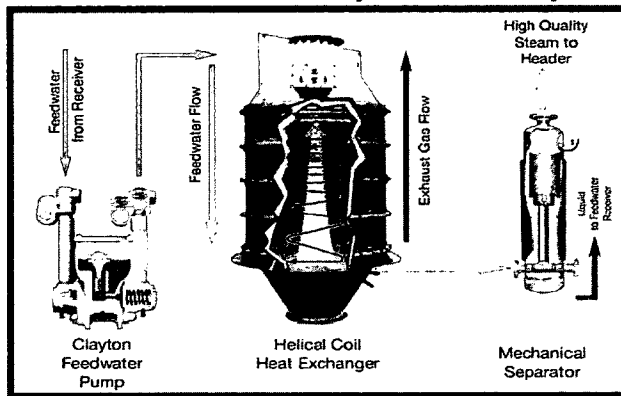
Figure 22. Helical coil WHRSG illustration. [36]

When NE Thermal the exhaust company evaluated the experimental results of this study they

indicated installing this on the G-oven afterburner stack would yield the lowest ROI of the set.

The corresponding steam produced by the WHRSG, G_{WHRSG} [kg/hr], will be between 543-542

kg/hr at 620.52 kPa based on the temperatures and flow rates measured in the G-oven afterburner

stack.[37] Table 10 shows the boiler steam generated and corresponding fuel consumed at

different loads and corresponding efficiencies as determined from the boilers manual (efficiency

refers to the fuel to steam efficiency of a boiler which is described by: combustion efficiency

equals the total heat released in combustion, minus the heat lost in the stack gases, divided by the

total heat released and fuel to steam efficiency is a measure of the energy converted to steam and

is equal to the combustion efficiency minus the percent heat losses through radiation and

convection).[30]

Table 10. Boiler specifications. [30]

Steam Generated (100% Load), $G_{100\%L}$ [kg/hr]	3,130
Steam Generated (46% Load), $G_{46\%L}$ [kg/hr]	1,435
Fuel Consumed (100% Load, 85% EFF), $FC_{100\%L,85\%EFF}$ [KWh]	2,308
Fuel Consumed (50%Load, 86% EFF), $FC_{50\%L,86\%EFF}$ [KWh]	1,140
Fuel Consumed (46% Load, Prorated EFF), $FC_{46\%LPR\%EFF}$ [KWh]	1,046

Note all steam is generated by the boiler at 620.5 kPa.

The fuel consumed at 50% Load and the corresponding 86% efficiency, $Q_{50\%L,86\%EFF}$, was calculated by scaling the 100% FC quantity at 85% efficiency by:

(38)

$$FC_{50\%L,86\%EFF} = \frac{85}{86} * FC_{100\%L,85\%EFF} * 0.5.$$

The fuel consumed at 46% load and a prorated efficiency based on the efficiency of other heat inputs near its loading, $FC_{46\%LPR\%EFF}$ was calculated by

(39)

$$FC_{46\%LPR\%EFF} = \frac{85}{86} * FC_{100\%L,85\%EFF} * G_{46\%L}/G_{100\%L}.$$

No measurements were made to substantiate the assumed steam flow rate or that the boilers operated at 46% load both were derived from the steam flow diagrams observed. [30] The boilers annual NG use without the supplementary steam from the steam generator, FC_{WHRSG}, was calculated by:

(40)

$$FC_{Boiler} = FC_{46\%LPR\%EFF} * O_{Boiler},$$

where O_{Boiler} is the hours of operation of the boiler. The resulting annual NG use reduction of the WHRSG, S_{WHRSG}, is calculated by:

(41)

$$S_{WHRSG} = (FC_{46\%LPR\%EFF} * O_{G-Oven}) * \frac{G_{WHRSG}}{G_{100\%L}}.$$

Note the operating hours of the G-oven are used because this system only generates steam while the G-oven is in operation. Table 11 shows the economic evaluation of the WHRSG option.

Table 11. Economic analysis G-oven afterburner WHRSG option.

	Boiler
Cost of System, TC_{WHRSG} [37]	$270,545
Incentive, I _{WHRSG}	$132,242
Actual System Cost, AC_{WHRSG}	$138,303-$138,495
Annual NG Use of the boiler (w/out WHRSG),FC _{Boiler} [MWh/year]	9,168
Annual NG Use Reduction of the boiler(w/ WHRSG), S _{WHRSG} [MWh/year]	1,937-1,934
Yearly Savings from NG Reduction (w/WHRSG), RV_{WHRSG} [USD/year]	$52,831-$52,754
ROI _{WHRSG} [years]	2.62-2.63

Preheat Air to Combustion Burners

The preheat air to combustion burners heat recovery option preheats the intake air of the NG burners using a plate heat exchanger (HX) shown schematically in Figure 23. Therefore the NG required to produce the flame temperature is decreased. Note this option was only considered on the G and J-oven afterburner stacks because they had the largest magnitude of waste heat emitted of the stacks measured in the study.
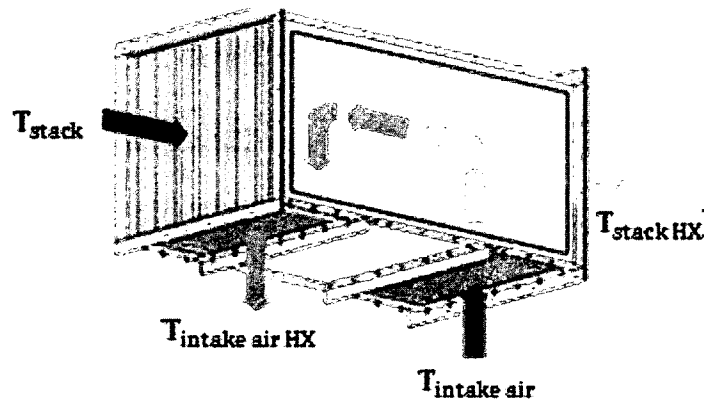

Figure 23. Plate heat exchanger. [38]

The intake air temperature, $T_{intake\ air}$ [K], was assumed to be 294 K (i.e., 21 C). Furthermore the exit temperature of both the stack, $T_{stack\ HX}$ [K], and intake air, $T_{intake\ air\ HX}$ [K], out of the HX and the heat transfer rate, $Z_{preheat}$ [KW], are unknown. These quantities can be determined from:

$$Z_{preheat} = UA \frac{(T - T_{stack\ HX}) + (T_{intake\ air\ HX} - T_{intake\ air})}{2} \quad (42)$$

$$Z_{preheat} = [\dot{m}_{stack}c_p(T_{stackHX} - T_{intake\ air})] \quad (43)$$

$$Z_{preheat} = -[\dot{m}_{stack}c_p(T_{intake\ air\ HX} - T)] \quad (44)$$

where U is the overall heat transfer coefficient, A [m^2] is the HX surface area, $\dot{m}$ [kg/s] is the

mass flow rate of the fluid in the stack, and c_p [J/kg-K] is the specific heat of the fluid in the

stack. The values $T_{stack\ HX}$, $T_{intake\ air\ HX}$, and $Z_{preheat}$ for a HX by Thermal Products are 713 K, 528

K, and 262-260 KW respectively for the G-oven data considering the flow traverse. Using this

information the annual NG savings, $S_{preheat}$ [MWh/yr], can be calculated by:

$$S_{preheat} = O * Z_{preheat}. \quad (45)$$

Again O is the annual hours of operation of the respective oven. Table 12 provides data of the

economic analysis for the preheat air recovery option.

Table 12. Economic analysis G and J oven preheat air.

	G-oven	J-oven
Cost of System, TC $_{preheat}$ [39-40]	$182,600	$149,250
Incentive, I $_{preheat}$	$87,561 – $86,892	$37,364
Actual System Cost, AC $_{preheat}$	$95,039 - $95,708	$111,886
Annual NG Use (w/out HX), FC $_{preheat}$ [MWh/year]	8,772	3,772
Annual NG Use Reduction (w/ HX), S $_{preheat}$ [MWh/year]	1,283 - 1,273	547
Yearly Savings from NG Reduction (w/ HX), RV $_{preheat}$ [USD/year]	34,634 - 34,370	14,779
ROI $_{preheat}$ [years]	2.74 -2.78	7.57

The NG flow-meter data recorders were not installed on the J-oven at Hitchiner. However it was known that the heat input into the J-oven is 43% of the G-oven. [27, 31] Therefore $R_{preheat}$, $S_{preheat}$, and $FC_{preheat}$ terms were scaled accordingly in Table 12.

Organic Rankine Cycle

The Organic Rankine Cycle (ORC) option converts waste heat captured by the organic fluid r245a into electricity by its expansion across an integrated power module generator as shown in Figure 24. This option would supplement the electricity purchased lowering the annual electricity usage.
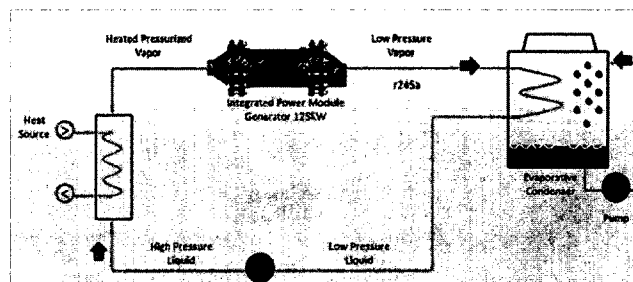
Figure 24. Illustration of the ORC thermodynamic cycle. [41]

The annual electricity use reduction that installing the ORC in the G-oven afterburner stack would lead to S_{ORC} is:

(46)

$$S_{ORC} = Z_{ORC} * O_{G-oven},$$

where Z_{ORC} is 110 KW. [42] Note the actual cost, AC_{ORC}, is a budgetary estimate that includes installation. [42] For this system no applicable financial incentives could be found. Although less energy was captured than the preheated air to the combustion burners and WHRSG option the yearly savings, RV_{ORC}, of the ORC is greater and this can be attributed to the higher cost of electricity with respect to natural gas. Table 13 shows the economic evaluation of the Calnetix ORC.

51

Table 13. Economic analysis G-oven afterburner ORC option.

	G-oven
Cost of System, TC_{ORC} [42]	$350,000
Incentive($0/MWh), I_{ORC}	$0.00
Actual System Cost, AC_{ORC}	$350,000
Annual Electricity Use Reduction, S_{ORC} [MWh/year]	539
Yearly Savings from Electricity Reduction (w/ORC), RV_{ORC} [USD/year]	64,627
ROI_{ORC} [years]	5.4

Building Heat

The building heat option uses a plate HX similar to the one shown in Figure 23 except the intake air that passes through the heat exchanger is blown into the building. This option lowers the amount of NG that would be used to heat the facility in the winter. Furthermore, in the summer no heat recovery will take place. Note a series of fans and controls would be installed to ensure that air delivered to different sections of the building is at the desired temperature set on the thermostat. Table 14 shows the results from the economic analysis of the building heat recovery option applied to the J-oven afterburner for a Munter's heat exchanger.

Table 14. Economic analysis J-oven afterburner building heat option.

	J-oven
Cost of System, $TC_{SpaceHeat}$ [43]	$84,000
Incentive, $I_{SpaceHeat}$	$17,881
Actual System Cost, $AC_{SpaceHeat}$	$66,318
Annual NG Use (w/out HX), $FC_{J\text{-}oven}$ [MWh/year]	3,772
Annual NG Use Reduction (w/ HX), $S_{SpaceHeat}$ [MWh/year]	262
Yearly Savings from NG Reduction (w/WHRSG), $RV_{SpaceHeat}$ [USD/year]	$6,180
$ROI_{SpaceHeat}$ [years]	11

It is not desirable to implement space heating in the G-oven afterburner stack because other options with lower ROIs can be applied.

Economizer

Note both boilers already have economizers on them. An economizer preheats the water entering the boiler harnessing waste heat of the boiler stack. Fig. 25 shows an economizer.
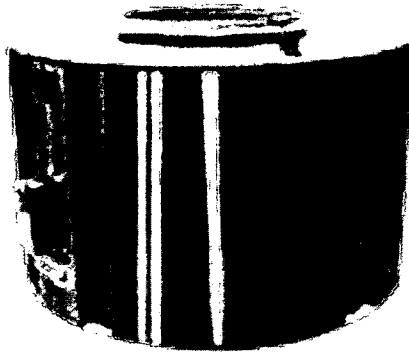
Figure 25. Economizer.[41]

The economizer can decrease the NG used by the boiler by 1%.[37] The annual NG use reduction with Economizer, S Economizer, was calculated by:

(47)

$$S_{Economizer} = 1\% * FC_{Boiler}.$$

Table 15 shows the details of installing an economizer on a boiler with an ROI of 7.4 years.

Table 15. Economic analysis boiler economizer option.

	Boiler
Cost of System, $TC_{Economizer}$[37]	$18,000
Incentive, $I_{Economizer}$	$4,560
Actual System Cost, $AC_{Economizer}$	$13,440
Annual NG Use (w/out Economizer), FC_{Boiler} [MWh/year]	9,168
Annual NG Use Reduction (w/Economizer), $S_{Economizer}$ [MWh/year]	67
Yearly Savings from NG Reduction (w/Economizer), $RV_{Economizer}$ [USD/year]	$1,822
ROI $_{Economizer}$ [years]	7.4

Thermo-electric

The thermo-electric option generates electricity from waste heat by the electrical phenomenon known as the Seebeck effect. In order to do this thermo-electric generators are installed inline the exhaust stack as shown in Figure 26. This option supplements electricity purchased lowering the annual electricity usage of the facility.

53
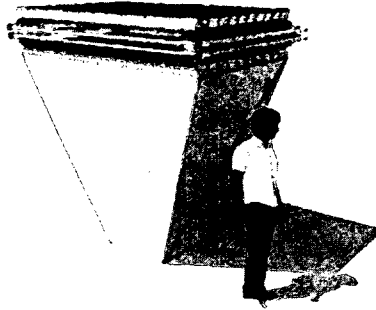
Figure 26. Thermoelectric electricity generator. [44]

The annual electricity use reduction S_{TE} was calculated by:

(48)

$$S_{TE} = Z_{TE} * O_{G-oven}.$$

where Z_{TE} is 2.9 KW for the temperatures and flow rates of the G-oven afterburner stack.[42] It was determined that 14 MWh/year of annual electricity generation could be displaced by installing this option with a corresponding annual savings of $1,700. No price was given by Alphabet energy the supplier, and it was not pursued by Hitchiner because of the more appealing savings of other recovery options. It is important to note more than 500 KW is exhausted from the G-afterburner stack and generating 2.9 KW is less than 1% of the available exhausted energy.

Combined Heat and Power

The combined heat and power (CHP) option generates electricity and reverts residual heat into the process (i.e., preheat combustion air, supplement steam to a boiler, or provide building heat). Figure 27 shows an illustration of a CHP system.

100%
Waste heat

NO fossil fuel

electricity

steam

Heat recovery
boiler

Backpressure
turbine generator

Figure 27. Illustration of a CHP system.[45]

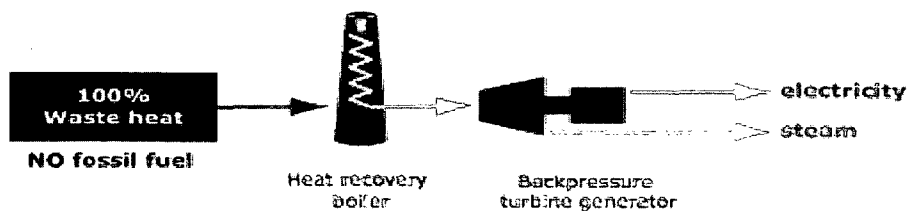Using the steam created by the heat recovery boiler in the exhaust stack a turbine generator creates the electricity. An analysis was performed for a set of turbines and heat recovery boiler that found and the maximum steam production using the G-oven afterburner is 1,360 kg/hr however a steam production of 13,608 kg/hr was necessary for it to be economical.[46-47]

Absorption Chillers

The absorption chillers option uses steam or hot water to drive the lithium bromide refrigeration cycle, which generates space cooling in the summer and space heating in the winter. Figure 28 shows a Trane absorption chiller.
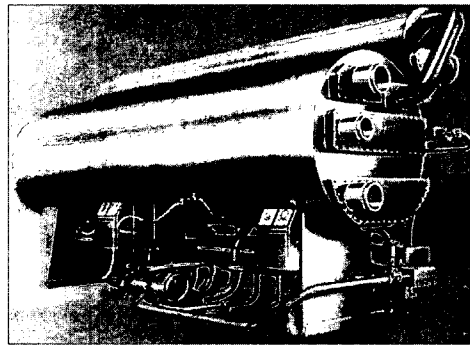
Figure 28. Absorption chiller.[48]

After considering the waste heat measurements Trane believed that absorption chilling was not economically feasible.[49]

Waste Heat Recovery Summary

The economics of the previously mentioned waste heat recovery options are summarized in Table 16. They are listed left to right in order of the lowest ROI at Hitchiner's current energy prices of $25.94/MWh delivered. No waste heat recovery options were found that could be feasibly applied to zones 2 and 3 of the G and J-oven due to the lower temperatures in these stacks (see Tables 9 and 10). Additionally, the emission of waste heat energy from the boiler

stack was too low for heat recovery options to be considered besides the economizer. There are 3

candidates for the G-afterburner stack, 2 for the J-afterburner stack, and 1 for the boiler stack.

However according to Hitchiner's standards which prefer an ROI of less than 2 years there are no

options. The only two options with ROIs near 2 years include, WHRSG and Preheat Air, which

would be applied in the G-oven afterburner stack. It is important to realize that only one option

can be chosen per stack.

Table 16. Summary of economic evaluations for heat recovery options based on NG price of $25.94/MWh.

Option	WHRSG	Preheat Air	ORC	Preheat Air	Space Heat	Economizer
Stack	G-AB	G-AB	G-AB	J-AB	J-AB	boiler
ROI [years]	2.62-2.63	2.74-2.78	5.4	7.57	11	7.4
Cost of System, TC	$270,545	$182,600	$350,000	$149,250	$84,000	$18,000
Yearly Energy Savings, RV	$52,831-$52,7541	$34,634 - 34,370	$64,627	$14,779	$6,180	$1,822
Energy Reduction, S [MWh/year]	1,937-1,934	1,283 - 1,273	539	547	262	67
Company	NE Thermal	ETTER	Calnetix	ETTER	Munter's	NE Thermal

Again any waste heat recovery option that has a ROI over 2 years is too long for Hitchiner to

consider. However based on fluctuations in the price of natural gas that Hitchiner has seen in the

past, the ROI can change as much as one year. Currently, Hitchiner is paying near its lowest

price for natural gas of $25.94/MWh delivered. In the past they have paid over $37.54/MWh.[15]

Furthermore, if production were increased from 24-4 for 51 weeks a year to 24-5 for 51 weeks a

year the ROI of the G-oven preheat air option and steam generation option would decrease to

between 2.11-2.13 and 1.59-1.60 respectively. Although, the ROIs of the options are not reduced

by the options associated carbon reduction within New Hampshire/United States Table 17 lists

the annual carbon reduction from each waste heat recovery option. Carbon reduction is

determined by the product of the annual energy saved [MWh/year] and the carbon content [metric tons/MWh] present in either NG or electricity.[50]

Table 17. Annual carbon reduction (7.18E-4 metric tons/KWh electricity and 1.7E-4 metric tons/KWh natural gas).

Annual Carbon Savings [metric tons/year]	
G-oven preheat	218
G-oven WHRSG	330
ORC	387
J-oven preheat	93
economizer	11
space heating	45

The G-oven WHRSG reduces the most carbon, followed closely by ORC and G-oven preheat technology. There is no financial incentive for carbon reduction.[51-52]

CHAPTER V

V. Previous Studies

Hitchiner Initial Study

An initial study in 2008 used a differential pressure Magnehelic gauge, Pitot-tube sensor, and a K-type thermocouple to measure dynamic pressure, to calculate flow, and measure temperature respectively. The initial study focused on the three stacks of the G-oven and the sensors were inserted at a height of approximately 1.40 meters (4.6 feet) from the roof-line. Note the insertion height of the new study was chosen to allow accurate comparison with the initial study. Thus, one of the reasons for the new study was to take measurements with equipment that would tolerate the stack conditions to produce more reliable measurements because the Magnehelic gauge has a temperature rating of 366 K (i.e., 93 C) and the temperature rating of the clear PVC tubing is only 313 K (i.e., 50 C). Both are far below the G-oven stack temperatures in Table 2.[15] The velocity calculation of the pitot-tube in this initial study is similar to that of the Eq. 5 used by the Accutube except that it doesn't have the B value and in this case the ΔP value is measured by the Magnehelic gauge. Furthermore the initial study calculated the density of the exhaust $\rho_{exhaust}$ by using Eqs. 17-20 together with two equations used to define the excess quantities of oxygen and nitrogen by:

$$O_{2,EA} = \frac{N_{2,combustion} + H_2O_{combustion} + CO_{2combustion}}{9}.$$

<div align="right">(49)</div>

and

<div align="right">(50)</div>

$$N_{2,EA} = O_{2,EA} \frac{\% \, Nitrogen}{\% Oxygen},$$

Instead of using a combustion analyzer's measurement of percent oxygen, $O_{2,Bacharach}$, to calculate the excess air, the initial study assumed the excess air was equal to 10% based on their familiarity with the oven, which is considerably different than the measured values in Table 4.

Different from the instantaneous measurements, the initial study made in the center and side of the stack and then averaged their values. The new study collected data continuously at the center of the stack in intervals of approximately 100 seconds for 24 hours a day, 7 days a week to create its average values. Also a profile across the stack cross-section was considered (see Fig. 18). This yielded a much larger and more representative data set from which to quantify the average temperature, volume flow rate, and waste heat emitted from the stack. Tables 18 shows the measured standard volume flow rate, stack temperature, and calculated waste heat loss from both the initial and new studies. Again, note the initial study was only performed on the stacks of the G-oven.

Table 18. Collected measurements from the initial and new studies.[15]

Parameter	Stack	Initial	New	% Diff
Volumetric Flow Rate, $\overline{Q}$ [SCMM]	A/B	74.33	56.95-55.72	26%-29%
	2	159.48	100.73	45%
	3	123.97	45.70	92%
Stack Temperature, $\overline{T}$ [K]	A/B	771	744	4%
	2	450	447	1%
	3	395	310	24%
Waste Heat Energy, $\overline{E}$ [KW]	A/B	717	576-516	22%-33%
	2	498	376	28%
	3	249	18	173%
Total Waste Heat Energy, $\overline{E}_{,total}$ [KW]		1,464	970-910	41%-47%

The measurements and calculated values from the initial study are greater than the values measured by the new study. Furthermore, there is a large difference between studies in their zone 3 measurements. Through talking with Hitchiner about the difference, it was determined that insulation had been inserted after the initial study into zone 3 to keep heat from passing through the stack. Altogether the initial measurements were not significantly different despite using less sophisticated sensors and obtaining a much smaller set of data points.

Furthermore, the opportunity of reusing the thermal energy in the G-oven Afterburner stack to preheat the combustion air was evaluated after the initial study as well. To this end mechanical contractors provided a cost estimate of $168,000 ± $25,000 for a heat exchanger system from Exothermics and installation.[15] A schematic of the system is shown in Fig. 29. The system was estimated to save 2,259 MWh/year.[15]
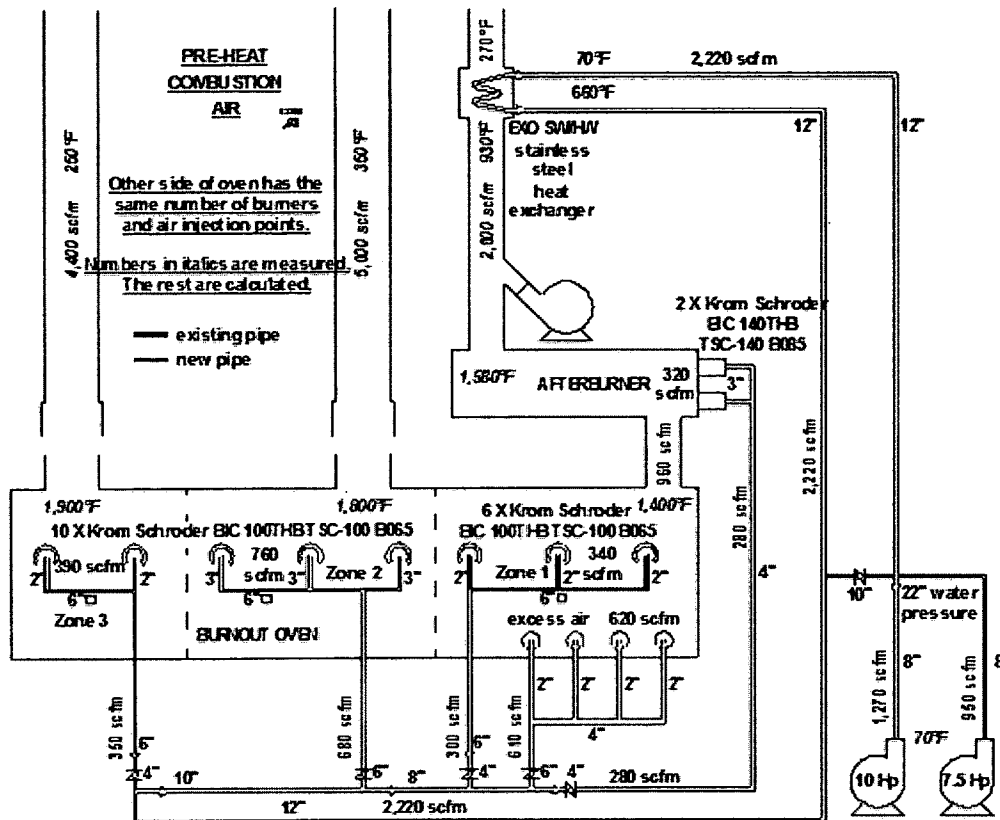
Figure 29. Schematic of waste heat recovery system from the initial study.[15]

Energy Resource Solutions Study

In 2010 Hitchiner's utility National Grid had the engineering firm Energy Resource Solutions (ERS) evaluate heat recovery options for its G-oven again. ERS's analysis assumed the oven has a single input of air and NG and exhausts through a single stack (i.e., the air exiting from the two other stacks of the oven was ignored). Figure 29 shows a circular draft inducer above the afterburner. This also was not accounted for in ERS's calculations. Thus their analysis comprised of a theoretical flow balance and was not substantiated by any direct measurements in the stack. Table 19 shows the G-oven Properties, Material Properties, Inferred Quantities, Measured Quantities, and Calculated Values used by ERS.

Table 19. Parameters used in ERS's analysis.[10]

Oven Properties	
HC $_{\text{G-oven,100\%L}}$ [MW]	3.75
HC $_{\text{G-oven, 50\%L}}$ [MW]	1.87
Material Properties	
Higher Heating Value of NG, HHV$_{\text{NG}}$ [KWh/kg]	14.98
Stoichiometric Air to Fuel Ratio, AFR$_{\text{stoch}}$ [kg$_{\text{air}}$/kg$_{\text{NG}}$]	17.2
Exhaust Density, ρ_{air} [kg/m^3]	1.20
Specific Heat, $c_{p,}$ [J/kg-K]	1,030
Inferred Quantities	
Firing Rate, FR	50%
Excess Air, EA	150%
Temperature of Air Exhausted to, T$_{\text{outsideair}}$ [K]	294
Temperature of Intake Air, T$_{\text{intakeair}}$ [K]	294
Measured Quantities	
Afterburner Exhaust Temperature, T$_{\text{stack}}$ [K]	944
Calculated Values	
Mass Flow of Natural Gas, M$_{\text{NG}}$ [kg/hr]	126
Mass Flow of Intake Air, M$_{\text{air}}$ [kg/hr]	5,427
Total Mass Flow, M$_{\text{total}}$ [kg/hr]	5,553
Exhaust Volume Flow Rate, Q$_{\text{stack,}}$ [m^3/min]	77
Annual Waste Heat, E [MWh/year]	4,615

The Total Heating Capacity HC $_{\text{G-oven,100\%L}}$ is listed in the oven manual its 50 % equivalent is scaled accordingly. In order to determine what firing rate the oven was operating at, current

loggers were implemented on the intake air blower of the oven thus tracking the motor amperage. By comparing the amperage of the blower to an amperage curve in the blower manual it was determined that the blowers were being operated at 50% load. Thus a 50% heat input load of the oven burners is the average. The "Material Parameters" in Table 19 are all constants of NG and its combustion with air. Note ERS assumed the exhaust density was equal to that of air at 294 K. The excess air values for both the boiler and ovens are assumed values that were not substantiated by any measurements. The G-oven afterburner exhaust temperature, T_{stack} [K] is the average temperature measured by a K-type thermocouple over two weeks of oven operation. The thermocouple was inserted in the afterburner exhaust stack between the exit of the afterburner and the circular draft inducer shown in Figure 29. The temperature of the air exhausted to, $T_{outsideair}$ [K], was arbitrarily selected by ERS to be 294 K. The mass flow of NG, M_{NG} [kg/hr], was calculated by:

(51)

$$M_{NG} = \frac{HC_{G-oven,50\%L}}{HHV_{NG}}.$$

The mass flow of the combustion air, M_{air}[kg/hr], was calculated by:

(52)

$$M_{intakeair} = (1 + EA) * M_{NG} * AFR_{stoch}.$$

The combined total mass flow of the air and NG, M_{total} [kg/hr], is a summation represented by:

(53)

$$M_{total} = M_{intakeair} + M_{NG}.$$

The standard volumetric flow rate of exiting the stack is:

(54)

$$Q_{total} = \frac{M_{total}}{\rho_{air}},$$

Again the waste heat, E, can then be calculated by Equation 15. Next calculating the energy savings from implementing a heat exchanger was performed by first calculating the term C_h [J/min-K] by:

$$C_h = M_{total} * c_{p,}$$

(55)

where c_p [J/kg-K] is the specific heat of air at standard conditions. Second, the term C_c [J/min-K] was calculated by:

$$C_c = M_{air} * c_{p,}$$

(56)

Third the thermal energy that the heat exchanger can extract, $Z_{preheat}$, [KW] was calculated by:

$$Z_{preheat} = e * C_c * (T_{stack} - T_{intake\ air}),$$

(57)

where the effectiveness, e, is a property of the specific heat exchanger (e.g., 34% for Munter's HX). Furthermore, the temperatures of the lowered exhaust stack temperature $T_{stackHX}$ [K] and the preheated air $T_{intakeairHX}$ [K] can be calculated by:

$$T_{stackHX} = T_{stack} - \frac{Z_{preheat}}{C_h},$$

(58)

$$T_{intakeairHX} = T_{intakeair} + \frac{Z_{preheat}}{C_c}.$$

(59)

The result of ERS's analysis on the preheat air of the combustion burners on the G-oven by installing a HX on the G-oven afterburner stack is that the HX is capable of extracting 1,524 MWh/year, making the new exhaust temperature 730 K and the preheated air temperature 518

64

K.[11] Table 20 shows the results of the economic analysis done by ERS for the preheat combustion air option.

Table 20. ERS's economic analysis.[10]

	G-oven (ERS)
Annual NG Use Reduction(w/ HX), S $_{preheat}$ [MWh/year]	1,524
Incentive($61.77/MWh)[7], I $_{preheat}$ [USD]	$ 100,000
Actual System Cost, AC $_{preheat}$ [USD]	$ 150,000
ROI $_{preheat}$ [years]	2.3

RISE Engineering Study

Again in 2011, RISE engineering evaluated the preheated combustion air option on the G-oven. Like ERS before them their analysis comprised of a theoretical flow balance and was not substantiated by any direct measurements in the stack. It was assumed the oven has a single input of air and NG and exhausts through a single stack (i.e., the air exiting from the two other stacks of the oven was ignored). Also the additional air from the circular draft inducer shown in Figure 29 was again ignored.

The operation manuals of the G-oven indicate intake air is supplied at 62.86 m^3/min under full load $Q_{intakeair,100\%L}$ and at 50% load the combustion air is simply 50% that of full load at 31.43 m^3/min $Q_{intakeair,50\%L}$. RISE assumed that the oven operated in "preheat" mode for 4 hours every week which caused the oven load to be 100%, and the remainder of the time the oven was "operational" with an oven load of 50%. Considering the calculations of energy savings, the corresponding mass flow rate of air M_{air} [kg/hr] is given by:

(60)

$$M_{air} = Q_{air}/v_{actual}.$$

where Q_{air} [m^3/min] is the volume flow rate of the intake air to the combustion burners, and v_{actual} [m^3/kg] is the specific volume of air. Temperatures, $T_{stackHX}$ [K]and $T_{intakeairHX}$ [K], are characteristic of Exothermics heat exchanger for the G-oven. The combustion efficiency $EFF_{combustion}$ is an assumed value. Lastly the annual energy savings $R_{Preheat}$, [MWh/year] is calculated by:

(61)

$$R_{Preheat} = \left(\frac{M_{intakeair} * c_{P.} * (T_{stack} - T_{stackHX})}{EFF_{combustion}}\right)_{Preheat}$$
$$+ \left(\frac{M_{intakeair} * c_{P.} * (T_{stack} - T_{stackHX})}{EFF_{combustion}}\right)_{Operational}$$

66

Table 21 and 22 summarize the values of the parameters used and the results of RISE's economic analysis respectively.[34]

Table 21. Parameters used in RISE's analysis.[53]

	Preheat	Operational
Oven Load	100%	50%
Volume Flow Rate of Air, Q_{air} [m³/min]	62.86	31.43
Specific Volume of Air, v_{actual} [m³/kg]	0.84	0.84
Mass Flow Rate of Air, M_{air} [lb/hr]	4,519	2,259
Specific Heat, c_p, [J/kg-K]	1030	1030
Temperature of Air leaving HX,$T_{stackHX}$ [K]	622	622
Temperature of Air Entering HX,T_{stack} [K]	294	294
Combustion Efficiency, $EFF_{combustion}$	0.82	0.82
Hours of Operation, O_{G-oven} [hours]	200	4,600
Annual Energy Savings, $S_{Preheat}$ [MWh/year]	100.41	1,154.62

Table 22.RISE's Economic Analysis.[53]

Annual NG Use Reduction(w/ HX), $S_{preheat}$ [MWh/year]	1,255
Incentive($61.77/MWh)[7], $I_{preheat}$ [USD]	$85,667
Actual System Cost, $AC_{preheat}$ [USD]	$96,933
$ROI_{preheat}$ [years]	2.8

Previous Studies Summary

Table 23 shows a summary of the results of the studies performed to date that have evaluated the recovery option of preheated combustion air on the G-oven (i.e., initial, ERS, RISE, and new).

Table 23. Summary of previous studies compared to new study.

	Initial[10] (2008)	ERS[15] (2010)	RISE[53] (2012)	NEW (2012)
Cost of System, $TC_{Preheat}$ [USD]	$193,000	$250,000	$182,600	$182,600
Annual NG Use Reduction (w/ HX), $S_{Preheat}$ [MWh/year]	2,259	1,524	1,255	1,283-1,273
Annual Savings from NG Reduction (w/ HX), $RV_{Preheat}$ [USD/year]	$ 60,744	$ 40,980	$ 33,746	$ 34,634- $ 34,370
Incentive, $I_{Preheat}$	$96,500	$104,028	$85,666	$86,892
Actual Cost, $AC_{Preheat}$	$96,500	$145,972	$96,934	$95,708
ROI $_{Preheat}$	1.6	3.6	2.9	2.74-2.78

Note the yearly savings from NG Reduction $RV_{preheat}$, the $ROI_{preheat}$, the incentive amount $I_{preheat}$, and actual cost $AC_{preheat}$ all reflect the 2012 rates of energy and incentives $26.89/MWh and $68.26/MWh respectively. Furthermore the studies performed by ERS and RISE are similar to one another in that they derived the annual NG use reduction by considering a single stream of air flow entering and exiting the oven without taking direct measurements in the exhaust stack. Also the initial and new studies are similar in that direct measurements in the exhaust stack were taken to determine the actual flow in the stack. However they differ because the initial study assumed a the oven operated at 100% firing rate where the NG flow sensors determined it operated at 48% on average. This means the flow rate of air into the burners is not as great as the initial study assumed. Thus reducing the corresponding heat that could be extracted from the same model HX.

CHAPTER VI

VI. CONCLUSIONS

In this research, the waste heat emitted from two ovens and a boiler used in the investment

casting manufacturing process by New Hampshire based Hitchiner Manufacturing Inc. Co. was

determined. This was achieved with measured temperature and standard volume flow rate data

both gathered from the exhaust stacks (i.e., three for each oven and one for the boiler) using a

thermal anemometer KURZ 2440. For these calculations, atmospheric pressure was assumed

which was confirmed using an Accutube differential pressure sensor. Also a combustion

analyzer sensor, Bacharach Fyrite Pro, was used to measure the volume percentage of oxygen

which was used to calculate the density of the exhaust. The exhaust density calculated from the

measurement does not vary more than 1.31% from the density of air. Thus within the accuracy

range of the pressure and density transducer it is possible the exhaust streams have the same

density as air and are at atmospheric pressure.

Whereas the density and pressure measurements were made instantly from a single measurement

taken once, the thermal anemometer collected data continuously over a period of one week per

stack (i.e., 24 hours a day for 7 days) in order to quantify the temperature and standard volume

flow rate of the exhaust. In order to support the KURZ sensor and protect its interface during the experiments, tripods and enclosures were designed, fabricated and implemented. The measurements obtained in the new study have similar results to an initial study that was performed by Hitchiner in 2008. By performing measurements over the course of a week, data was gathered in the new study to more accurately quantify the average temperature, volume flow rate, and waste heat emitted during operation.

The data acquired in the new study along with assumptions for the process allowed several waste heat recovery options to be assessed with respect to the waste heat recovered, energy saved, and return on investment. Based on the nine waste heat recovery options considered, none of them have a ROI less than 2 years as Hitchiner requires. However, pre-heating the combustion air of the burners and generating steam to supplement the boilers using the exhaust of the G-oven afterburner stack are both comparable having maximum ROIs of 2.78 and 2.63 years respectively with a 24/4 schedule of operation. Based on their ROIs is recommended the waste heat recovery steam generator be installed because it has the lowest ROI.

APPENDICES

APPENDIX I: LIST OF REFERENCES

[1] United Nations Industrial Development Organization (2009) "Policies and Measures to Realize Industrial Energy Efficiency and Mitigate Climate Change" Web. 16. Feb. 2011. <http://www.unido.org/index.php?id=1000596>.

[2] Natural Resources Canada, ecoENERGY (2008) "Energy Use in the Canadian Manufacturing Sector". Web. 17 Feb. 2011. <http://publications.gc.ca/site/eng/375377/publication.html>

[3] U.S. Energy Information Administration: Independent Statistics and Analysis (2009) "SEDS State Energy Data System New Hampshire" <http://www.eia.gov/state/seds/seds-states.cfm?q_state_a=NH&q_state=New%20Hampshire>

[4] ICF International. "Metal Casting." *U.S. Environmental Protection Agency: Energy Trends in Selected Manufacturing Sectors: Opportunities and Challenges for Environmentally Preferable Energy Outcomes* 1 (2007): 3-65,3-70. <www.epa.gov/sectors/pdf/energy/report.pdf.> Web. 30 Jan. 2011.

[5] U.S. Department of Energy: Energy Efficiency and Renewable Energy. "Largest Producer of Steel Products in the United states Achieves Significant Energy Savings at its Minntac Plant." *Industrial Technologies Program: Save Energy Now* 1 (2008): 1-4. Web. 2 Feb. 2012. <http://www1.eere.energy.gov/manufacturing/tech_deployment/case_studies.html>

[6] U.S. Department of Energy: Energy Efficiency and Renewable Energy. "Waste Heat Reduction and Recovery for Improving Furnace Efficiency Productivity and Emissions Performance." *Industrial Technologies Program: A Best Practices Process Heating Technical Brief* (2004): 1-10. Web. 1 Feb. 2012. <http://www1.eere.energy.gov/>

[7] Monte. "Waste Heat Recovery in a Coffee Roasting Plant." *Applied Thermal Energy* 1 (2003): 1-8. *Elsevier Science Ltd..* Web. 1 Feb. 2012.

[8] U.S. Department of Energy: Energy Efficiency and Renewable Energy. "Save Energy Now Assessment Helps Expand Energy Management Program at Shaw Industries." *Industrial Technologies Program: Save Energy Now* 1 (2008): 1-4. Web. 2 Feb. 2012. <http://www1.eere.energy.gov/manufacturing/tech_deployment/case_studies.html>

[9] J.A. Schey. "Introduction to Manufacturing Processes." 3d. ed., McGraw-Hill 2000. Print. 20 March. 2012.

[10] *Energy Study prepared for Hitchiner Manufacturing Co, Inc. Milford, NH audit sponsored by National Grid.* North Andover: Energy & Resource Solutions, 2010. Print. 13 Apr. 2011.

[11] "NextEra Energy Resources." *Next Era Energy Resources*. N.p., n.d. Web. 29 Sept. 2012. <http://www.nexteraenergyresources.com/what/nuclear_seabrook.shtml>.

[12] "How much electricity does an American home use? - FAQ - U.S. Energy Information Administration (EIA)." *U.S. Energy Information Administration (EIA)*. N.p., n.d. Web. 29 Sept. 2012. <http://www.eia.gov/tools/faqs/faq.cfm?id=97&t=3>.

[13] Hitchiner Manufacturing Co., Inc. (2011), "An Introduction to the Investment Casting Process," www.hitchiner.com. Web. 4 March 2011.

[14] "Waste Heat Recovery: Technology and Opportunities in the U.S. Industry." *U.S. Department of Energy Industrial Technology Program* 1 (2008): 1-68. Print.

[15] Farkas, Attila . *Energy Recycling from ACF's Burnout-Oven*. Milford: Hitchiner Manufacturing Inc., Co., 2008. Print. 13 Apr. 2011.

[17] *Series 2440 Portable Thermal Anemometer User's Guide*. 5 ed. Monterey, CA: KURZ Instruments, Inc., 2000. Print. 1 May. 2011.

[18] *Model 2445 High Temperature Portable Air Velocity Meter*. Monterey, CA: KURZ Instruments, Inc., 2000. Print. 1 May. 2011.

[19] *General Specifications EJX910A Multivariable Transmitter*. 6 ed. Tokyo, Japan: Yokogawa Electronics, 2006. Print. 1 May. 2011.

[20] "Accutube." *Meriam Process Technologies | Welcome!*. N.p., n.d. Web. 3 Jan. 2012. <http://www.meriam.com/productcart/pc/viewCategories.asp?idCategory=16>.

[21] MERIAM INSTRUMENTS. "DERIVATION OF ACCUTUBE FLOW EQUATION." *FLOW HANDBOOK for MERIAM ACCUTUBE* 1 (2002). Print. 12 May. 2011.

[22] Kurz, Jerry. "Kurz, Jerry 'Characteristics and applications of industrial thermal mass flow transmitters." *Instrumentation for the Process Industries* - (1992): 107-113. Print. 20 Jan. 2012.

[23] Incropera, Frank P., and David P DeWitt. *Introduction to heat transfer*. 4th ed. New York ; Toronto: J. Wiley, 2002. Print.

[24] Borgnakke, C., Richard Edwin Sonntag, and Gordon J. Wylen. *Fundamentals of thermodynamics*. 7th ed. New York, NY: Wiley, 2009. Print. 2 Feb. 2011.

[25] Kent, William. *Mechanical engineers' handbook;*. 12th ed. New York, NY: Wiley, 1950. Print. 13 Apr. 2011.

[26] TSI. "Combustion Analysis Basics: An Overview of Measurements Methods and Calculations Used in Combustion Analysis." *Combustion Analysis* - (2004): 1-35. Print. 1 Aug. 2011.

[27] Myers, Norm . *G-Oven*. Bristol, CT: Etter Engineering. Print.

[29] Fox, Robert W., Alan T. McDonald, and Philip J. Pritchard. *Introduction to Fluid Mechanics*. 7 ed., Internat. ed. Hoboken, NJ: Wiley, 2011. Print. 20 Jan. 2012.

[30] "Clayton Industries :: SigmaFire Boilers." *Steam Boiler | Steam Generator | Clayton Industries*. N.p., n.d. Web. 17 Jan. 2011. <http://www.claytonindustries.com/clayton

[31] Myers, Norm . *J-Oven*. Bristol, CT: Etter Engineering. Print.

[36] "Clayton Industries:: Literature." *Steam Boiler | Steam Generator | Clayton Industries*. N.p., n.d. Web. 3 Jan. 2012. <http://claytonindustries.com/clayton_lt1_literature.aspx>.

[38] "Exothermics - Heat Exchanger & Heat Recuperator - Buy HERE!." *Power Equipment Company - Gas Burners, Vaporizers, Combustion Equipment*. N.p., n.d. Web. 3 Jan. 2012. <http://www.peconet.com/Products/exotherm.htm>.

[39] Myers, Norm. "G-Oven Recuperation Upgrade." *MM-101117 Hitchiner -G-Oven Recuperation Upgrade* 1 (2011): 7. Print. 1 Dec. 2011.

[40] Myers, Norm. "J-Oven Recuperation Upgrade." *MM-101125 Hitchiner -J-Oven Recuperation Upgrade-2* 1 (2011): 7. Print. 1 Dec. 2011.

[41] "Calnetix | Innovation That Drives Industries." *Calnetix | Innovation That Drives Industries*. N.p., n.d. Web. 3 Jan. 2012. <http://www.calnetix.com/>.

[44] "Alphabet Energy. Thermoelectrics for waste heat recovery.." *Alphabet Energy. Thermoelectrics for waste heat recovery.*. N.p., n.d. Web. 9 Mar. 2012. <http://www.alphabetenergy.com/>.

[45] Recycling Energy with Cogeneration | RED | Recycled Energy Development." *Recycling Energy with Cogeneration | RED | Recycled Energy Development*. N.p., n.d. Web. 3 Jan. 2012. <http://www.recycled-energy.com/>.

[48] "Chiller Systems - Direct-Fired Absorption Chillers - Absorption Liquid Chillers | Trane." *TRANE Air Solutions - Air Conditioners, Heat Pumps, HVAC Systems, Furnaces, Thermostats - Commercial and Residential*. N.p., n.d. Web. 3 Jan. 2012. <http://www.trane.com/Commercial/DNA/View.aspx?i=1036>.

[50] "Calculations and References | Clean Energy | US EPA." *US Environmental Protection Agency*. N.p., n.d. Web. 9 Dec. 2012. <http://www.epa.gov/cleanenergy/energy-resources/refs.html>.

APPENDIX II: EMAIL/PHONE CORRESPONDENCES

[16] Hutchinson, Kim. "Stacks." Email to Patrick T. Kilar.13 Apr. 2011.

[28] Myers, Norm. "Norm Myers." Email to Patrick T. Kilar and Jillian Tombarelli. 16 Dec. 2011.

[32] Tombarelli, Jillian. "new natural gas price." Email to Patrick T. Kilar. 2 Dec. 2011.

[33] Hess, David. Telephone call about NH Pay for Performance Program. 11 Nov. 2011.

[34] Krey, Robert. "Hitchiner Energy Savings" Email to Patrick T. Kilar.10 Nov. 2011.

[35] Lagasse, Ryan. "Incentive." Email to Jillian Tombarelli and Patrick T. Kilar. 20 Dec. 2011.

[37] Elliot, John. "NHIRC Waste Heat Recovery Project: July 15, 2011." Email to Patrick T. Kilar.15 Jul. 2011.

[42] Miller, Bob. "heat." Email to Patrick T. Kilar. 19 Oct. 2011.

[43] Worachek, Chris. "MEGTEC Systems Proposal 17307 for Heat Recovery." Email to Patrick T. Kilar. 27 Oct. 2011.

[46] Munson, Dick. "Contact for submission from RecycledEnergy.com." Email to Patrick T. Kilar. 13 Oct. 2011.

[47] Kempland, Dan. "Turbosteam." Email to Patrick T. Kilar. 18 Oct. 2011.

[49] Vecchione, Nick. "Hitchiner Manufacturing." Email to Patrick T. Kilar. 10 Nov. 2011.

[51] Ruderman, Jack. "RGGI." Email to Patrick T. Kilar. 02 Nov. 2011.

[52] DeVito, Lisa. "Carbon Credits." Email to Patrick T. Kilar. 02 Nov. 2011.

[53] Lagasse, Ryan. "Calculations." Email to Jillian Tombarelli and Patrick T. Kilar. 6 Mar. 2012.

[54] Hutchinson, Kim. "ACF Facility Layout." Email to Patrick T. Kilar. 3 Mar. 2011.

G Afterburner Zone

Notes: Data acquisition on the G-oven afterburner stack spanned Monday-Friday. First dip in data (see Fig. A-1) is due to oven shutdown due to lack of product according to Plant Manager (Mike McNamara). Second dip is due to planned shutdown at the end of the production week. No data was taken over the weekend because of hurricane Irene. Flow rate possibly increased because inducer above afterburner was left on and no shells in the oven allowed the air to flow unobstructed from the oven.
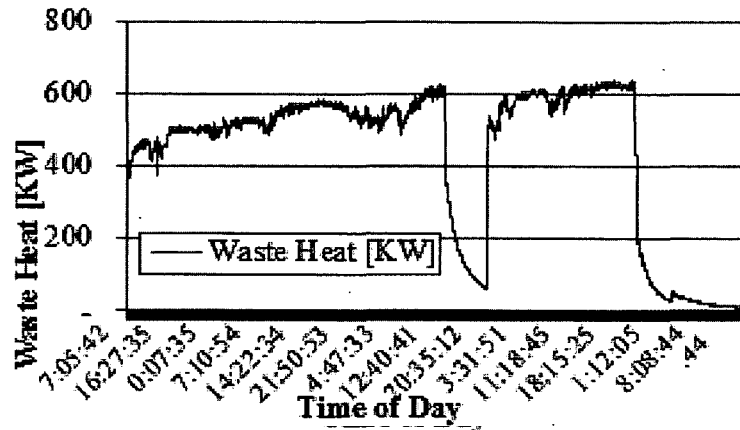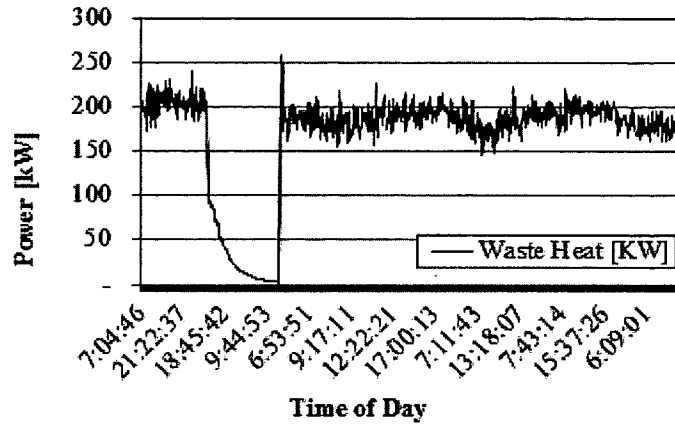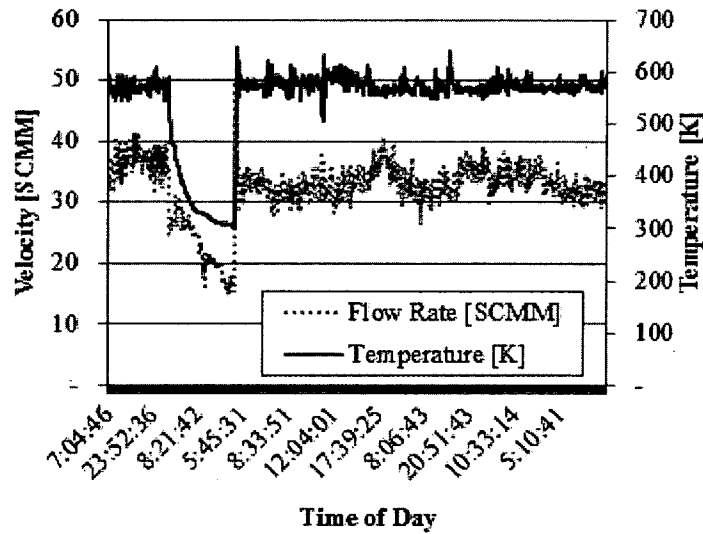
Figure 30. Waste heat emitted from G-oven afterburner stack.
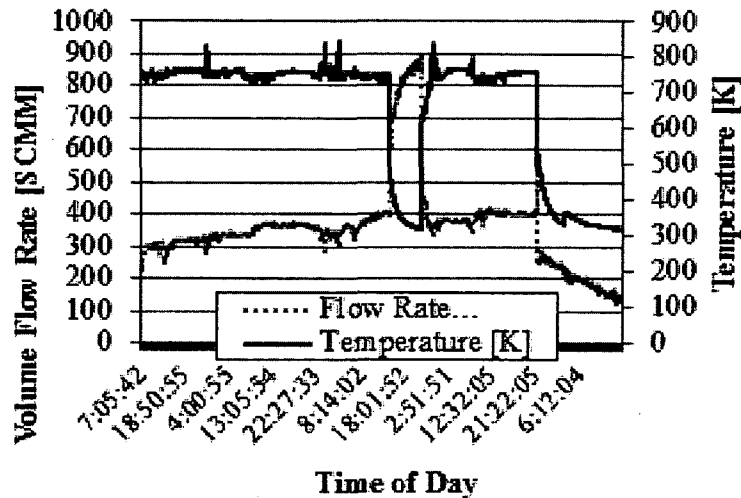
Figure 31. Standard volume flow rate and temperature from G-oven afterburner stack.

G Zone 2

Notes: Data acquisition began on Monday. First dip is due to oven shutdown due to lack of product. Flow and temperature decrease uniformly over shutdown. This stack has no inducer to blow in it. The second dip is due to the weekend shutdown.
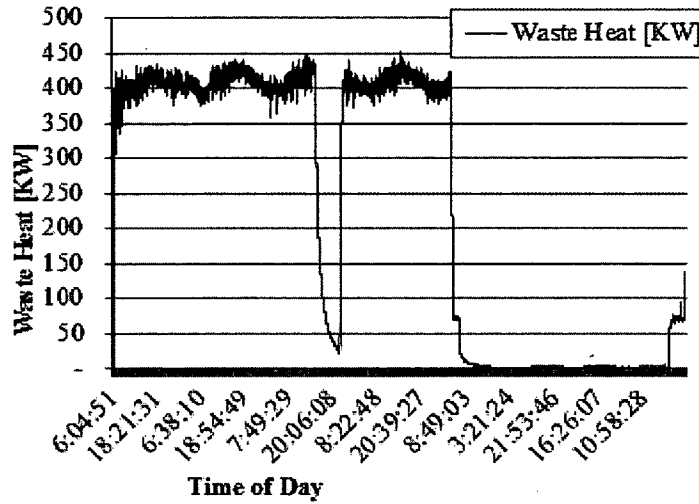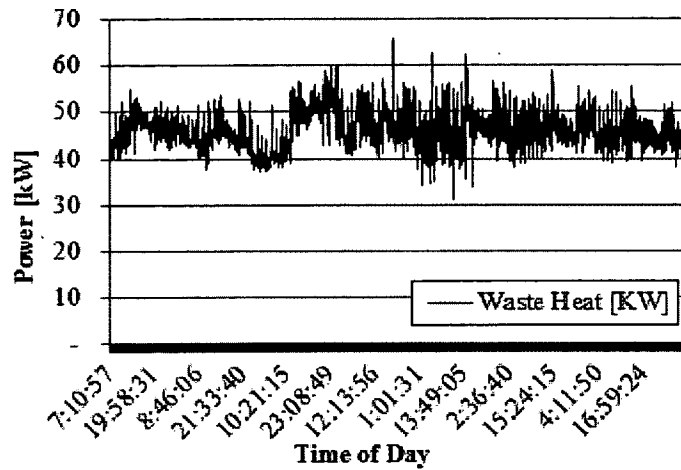

Figure 32. Waste heat emitted from G-oven zone 2 stack.
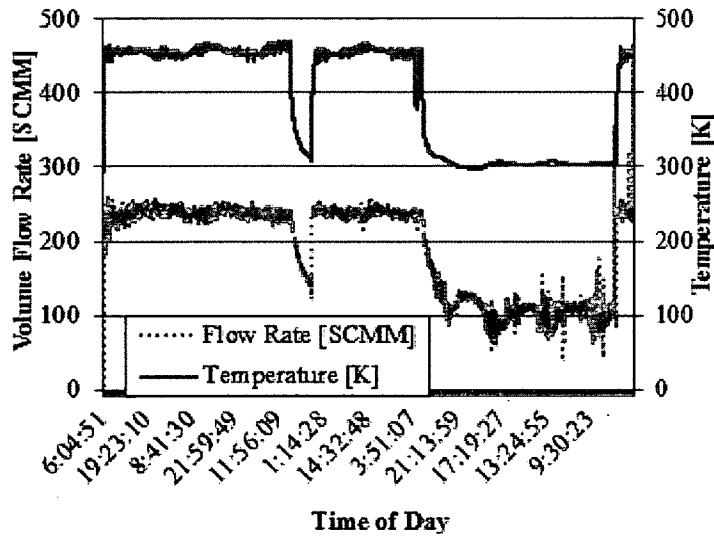
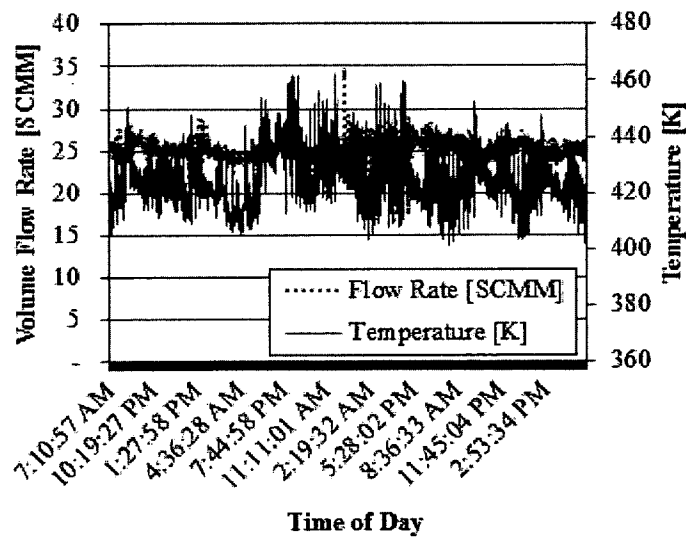**Figure 33.** Standard volume flow rate and temperature G-oven zone 2 stack.

76

G Zone 3

Notes: Data acquisition began on Monday. Spikes in data are single data point scatter.
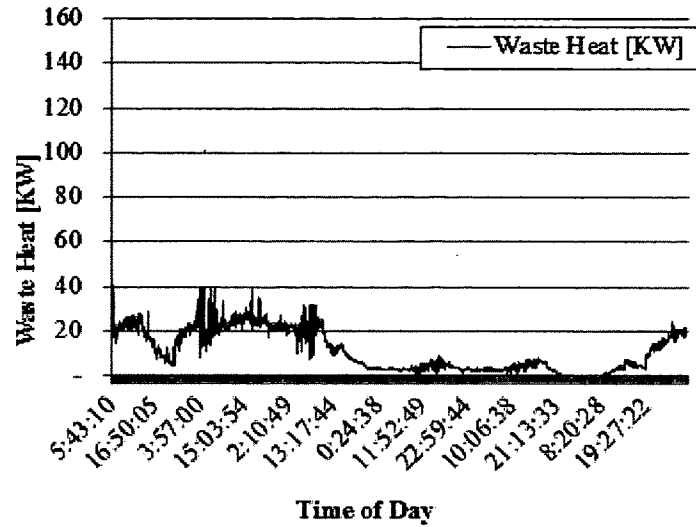
Figure 34. Waste heat emitted from G-oven zone 3 stack.
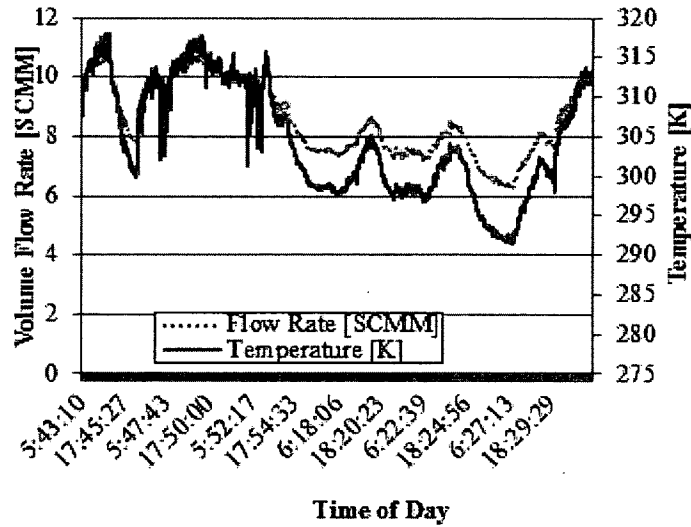
Figure 35. Standard volume flow rate and temperature G-oven zone 3 stack.

J Afterburner Zone

Notes: Data acquisition began on Thursday. First dip is due to weekend shutdown. Large spike in data is a single data point scatter.

Figure 36. Waste heat emitted from J-oven afterburner stack.

Figure 37. Standard volume flow rate and temperature J-oven afterburner stack.

Notes: Data acquisition began on Monday. Oven was run over the weekend with no lack of product.

Figure 38. Waste heat emitted from J-oven zone 2 stack.

Figure 39. Standard volume flow rate and temperature J-oven zone 2 stack.

J Zone 3

Notes: Data acquisition began on Thursday. First dip is due to weekend shutdown. The oven was run with a lack of product thus it was not fired constantly throughout the day (i.e., square wave like features).
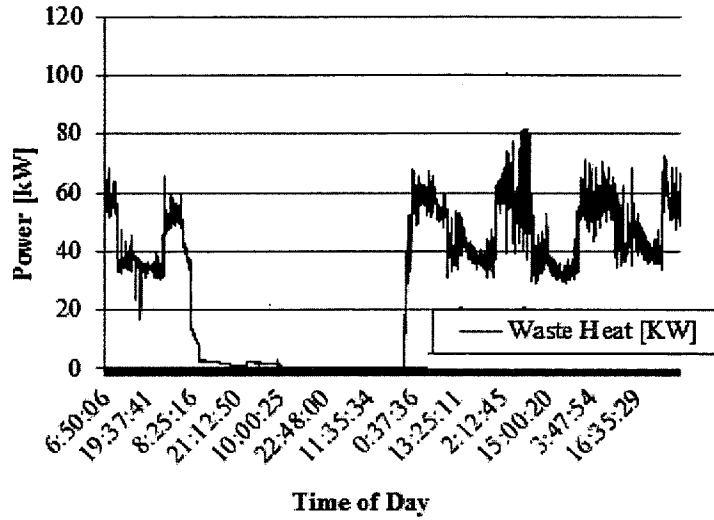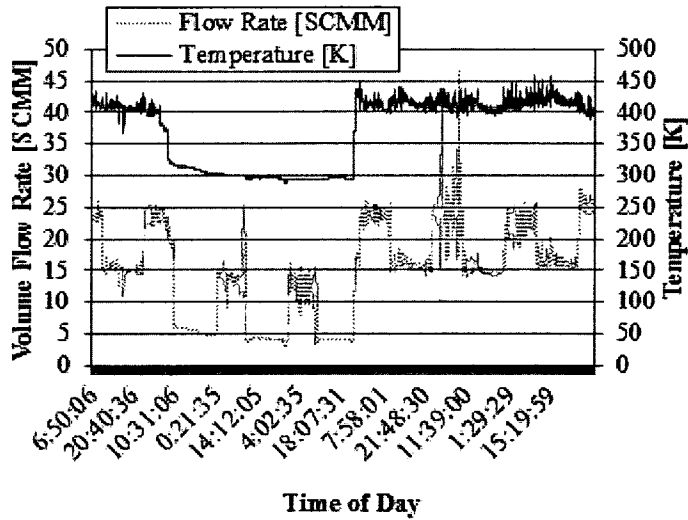

Figure 40. Waste heat emitted from J-oven zone 3 stack.

Figure 41. Standard volume flow rate and temperature from J-oven zone 3 stack.

80

Boiler

Notes: Data Acquisition began on Monday. Boiler was in Lag control strategy on Tuesday (first large valley). During the middle of the day Wednesday it began Lead control. This "Lead-Lag" control scheme causes the fluctuations in the data.
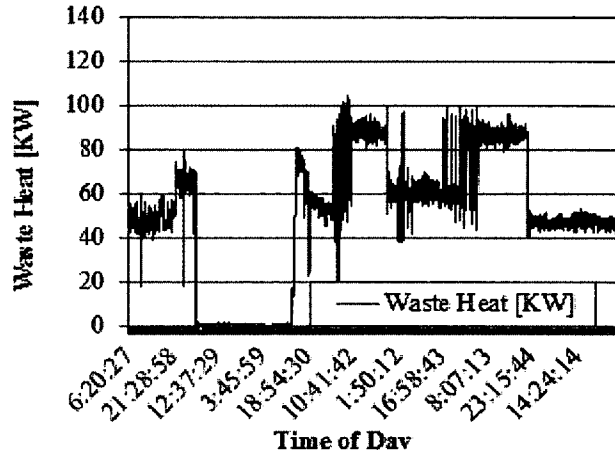

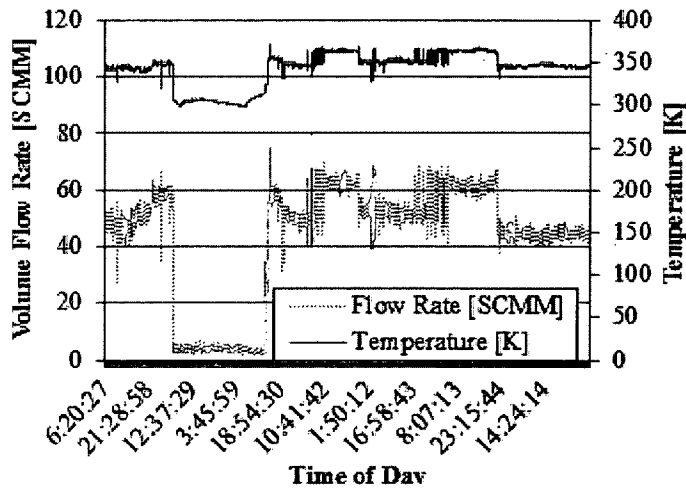Figure 42. Waste heat emitted from boiler stack.

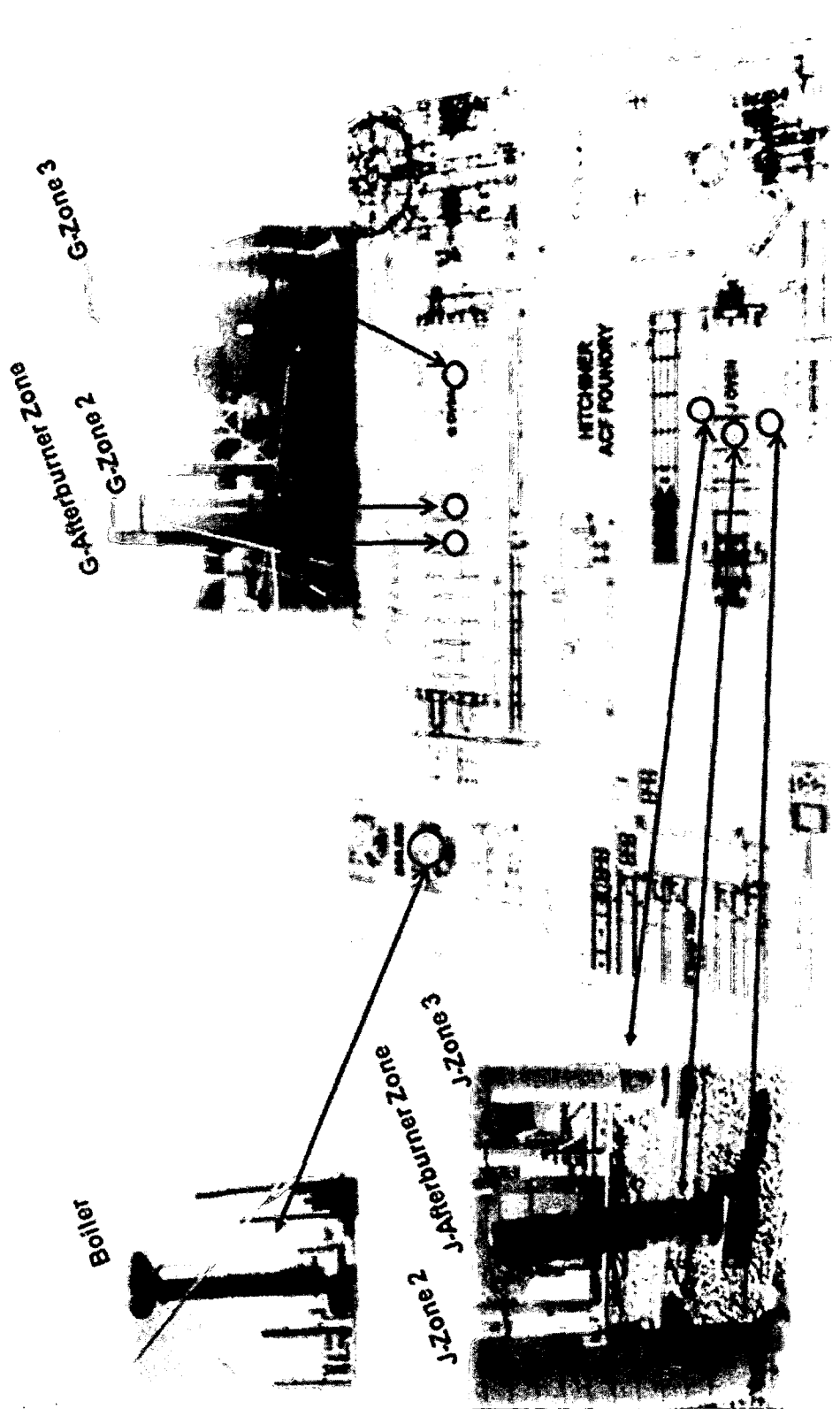Figure 43. Standard volume flow rate and temperature boiler stack.

Figure 44. ACF floor layout.[54]

82